MODELLING THE FILL-AND-SPILL DYNAMICS AND WIDLFIRE IMPACTS ON THE HYDROLOGICAL CONNECTIVITY OF EPHEMERAL WETLANDS IN A ROCK BARRENS LANDSCAPE

MODELLING THE FILL-AND-SPILL DYNAMICS AND WIDLFIRE IMPACTS ON THE HYDROLOGICAL CONNECTIVITY OF EPHEMERAL WETLANDS IN A ROCK BARRENS LANDSCAPE

By GREGORY J. VERKAIK, Hons B.Sc.

A Thesis Submitted to the School of Graduate Studies in Partial Fulfillment of the Requirements

for the Degree of Master of Science

McMaster University

MASTER OF SCIENCE (2021)

McMaster University

School of Earth, Environment & Society

Hamilton, Ontario, Canada

TITLE: Modelling the fill-and-spill dynamics and wildfire impacts on the hydrological connectivity of ephemeral wetlands in a rock barrens landscape

AUTHOR: Gregory J. Verkaik, Hons. B.Sc. (McMaster University)

SUPERVISOR: Dr. James M. Waddington

NUMBER OF PAGES: xiv, 86

LAY ABSTRACT

Rock barrens landscapes provide several important ecosystem services, which are influenced by hydrological flow paths and water storage on the landscape. Central to these hydrological dynamics is the storage and discharge of water in small wetlands which form in bedrock depressions. Here we develop a simple hydrological model to simulate the water storage and discharge of rock barrens wetlands. We then use this model to explore how wildfire disturbance is likely to change the supply of water to the rest of the landscape by simulating several different scenarios and testing which changes in the model have the largest impact on the water supply. We show that wetlands discharge more water after wildfire disturbance, mainly because of increases in run-off from areas upstream of the impacted wetlands. This modelling approach helps us better understand how wildfire is likely to impact the ecosystem services of a rock barrens landscapes.

ABSTRACT

Ontario's rock barrens landscape consists of exposed bedrock ridges which host a mosaic of thin lichen- and moss- covered soil patches, forested valleys, beaver ponds, and depressional wetlands. Peat-filled ephemeral wetlands within bedrock depressions act as gatekeepers to hydrological connectivity between their small headwater catchments and the rest of the landscape downstream through strong fill-and-spill dynamics. We developed a water balance model, RHO, with inputs of precipitation and potential evapotranspiration (PET) to better understand the factors impacting water table (WT) and storage dynamics and in turn the hydrological connectivity of ephemeral wetlands. Field surveys were conducted at six wetlands to obtain and determine the variability in measurable site characteristics, in particular the wetland depression morphometry, to parameterize RHO. Three sites were used in a calibration and validation procedure where modelled WTs were compared to measured WT data from the snow-free seasons for each site to determine the best parameter values. We show that RHO is capable of predicting WT dynamics with inputs of precipitation and PET, when parameterized for specific sites.

Wildfire disturbance is known to increase the run-off from hillslopes and remove surface organic soils through combustion. To predict the impacts of wildfire disturbance on ephemeral wetland hydrological connectivity, a generic model wetland depression was parameterized in RHO and used to predict the changes in hydrological connectivity under various wildfire scenarios and test the sensitivity of modelled connectedness to impacted parameters. Modelled results show that connectivity increases under all scenarios tested, and that changes to connectivity are primarily due to increases in run-in.

Water balance models, like RHO, can be used to better understand the hydrological connectivity of wetlands in a rock barrens landscape. These models are useful in predicting impacts

on the hydrological connectivity, and hydrological ecosystem services, from disturbances such as wildfire and can inform future field research experimental designs.

ACKNOWLEDGEMENTS

I would like to thank Dr. Mike Waddington for his supervision and guidance throughout my entire early research career. His expertise and helpful direction have helped make this research project possible. Thanks for always encouraging thoughtful discussion and helping when things felt overwhelming, and especially for giving up your time to hold branches out of the way while surveying sites. I look forward to continuing as your student in my PhD.

I thank Dr. Sophie Wilkinson for being a continued pillar of support and always giving up your time to help when I felt lost. I would not have made it through these two (plus) years without your mentorship and caring friendship. Thank you for putting up with me through it all.

To Dr. Paul Moore, thank you for all the time and effort put into getting RHO up and running, I can only hope to have your MATLAB skills someday. I'd like to thank Drs. Chantel Markle and Colin McCarter for all your helpful comments on my (often very long) updates, and always contributing insights whenever needed.

I'd like to thank the members of 317C, Danielle Hudson, Taylor North, and Renée McDonald for being such a great group of friends and fellow MSc students. I've deeply missed our (constant) chatting in the office pre-covid and will always remember our "writing retreat" to Florida. Thank you for your support and friendship. Thanks to the rest of the McMaster Ecohydrology Lab, past and present, all of whom have been a wonderful group of researchers that I am lucky to call my colleagues.

To my parents for always giving when needed and supporting me throughout my academic career, thank you. And thank you to my siblings for being there through thick and thin. Finally, thank you to Gracie and Zayn, my little niblings, for being two wonderful gifts of joy during such difficult times, I'm so happy to be your uncle.

TABLE OF CONTENTS

LIST OF FIGURES

LIST OF TABLES

LIST OF ABBREVIATIONS AND SYMBOLS

DOB	Depth of burn
ET	Evapotranspiration
HRU	Hydrological response units
P	Precipitation
PET	Potential Evapotranspiration
p-shape	Depression morphometry parameter
$\mathbf{Q_{in}}$	Run-in from upslope watershed
$\mathbf{Q_{out}}$	Discharge from wetland
RHO	Rock-barrens Hydrology with Organics model
RMSE	Root mean squared error
Sy	Specific yield
WT	Water Table

DECLARATION OF ACADEMIC ACHIEVEMENT

This thesis has been prepared in the traditional format, with a single manuscript including introduction, methods, results, discussion, and conclusion. This thesis has been written by the author, under the supervision of Drs. James M. Waddington, Sophie L. Wilkinson, and Paul A. Moore, who all provided guidance in research design, data analysis, and writing. Dr. Paul A. Moore contributed significantly to the development of the model, RHO, used in this thesis. Data collection was carried out primarily by the author with assistance from other members of the McMaster Ecohydrology Lab, in particular Taylor North, and Drs. Sophie L. Wilkinson and James M. Waddington.

CHAPTER 1: INTRODUCTION

The hydrological regime of a watershed has a direct impact on the ecosystem form and function and ecosystem services and, as such, developing metrics for assessing the hydrological regime of a watershed have long been at the forefront of ecohydrological research. For example, hydrological connectivity is a topic which has been given much attention within watershed science over the past few decades as a way of describing the flow of water through a watershed and the connection between elements of the landscape (*e.g.*, Ali et al., 2018; Bracken & Croke, 2007; Branfireun & Roulet, 1998; Frisbee et al., 2007; Oswald et al., 2011; Pringle, 2001, 2003; Spence & Phillips, 2015). The patterns of hydrological connectivity of upstream landscape elements, or hydrological response units (HRUs; Flügel, 1995) determine the supply of water, along with nutrients, sediment, and other chemical and biological components, to various downstream HRUs, therefore also influencing the ecological connectivity of the landscape (Bracken & Croke, 2007). The supply of water to an HRU thus has a large control its patterns of connectivity in addition to the unit's ability to support various flora and fauna and provide ecosystem services. Thus, impacts to the patterns of hydrological connectivity from disturbances, such as wildfire, on the landscape have implications for the ecosystems which a landscape supports and have the potential to cause significant changes to the ecological functioning of a watershed.

Wildfire impacts the landscape by combusting above-ground vegetation and organics from the upper layers of the soil profile. The removal of vegetation in turn increases erosional processes often further removing soil from hillslopes (Moody et al., 2013). A reduction in soil organic content and soil depth can have profound impacts on soil hydrophysical properties (Thompson & Waddington, 2013), typically reducing infiltration capacity and runoff thresholds through the reduction in soil water storage potential (*e.g.*, Beatty & Smith, 2013; Bladon et al., 2014; Ebel et al., 2012; Hallema et al., 2018; Neary et al., 2000; Robinne et al., 2020; Silins et al., 2009) and reducing the specific yield (Sy; the amount of water removed from a soil for a given change in water table (WT) position; Price, 1996) of soils (Sherwood et al., 2013). Wildfire is also known to induce chemical changes to soils creating hydrophobic layers which further reduce infiltration capacity and increase runoff following wildfire (Beatty & Smith, 2013; Doerr et al., 2000; Shakesby et al., 2000).

While the hydrology of some Canadian Shield landscapes has been the focus of many studies (*e.g.,* Allan & Roulet, 1994; Branfireun & Roulet, 1998; Frisbee et al., 2007; Oswald et al., 2011; Spence & Woo, 2008), the hydrology of smaller depressional peatlands and ephemeral wetlands on Ontario's rock barrens landscape has been the subject of fewer studies (Didemus, 2016; Moore et al., 2021). Moreover, wildfire and its impacts on surface hydrology has been greatly studied in many other landscapes around the world and Canada (*e.g.,* Bladon et al., 2014; Bond-Lamberty et al., 2009; Shakesby et al., 2000; Silins et al., 2016), but the impacts of wildfire on the thin soil deposits and peat-filled depressions of rock barrens landscapes have not been studied, possibly due, in part, to the rare occurrence of wildfire in this region (Alexander, 1980; Van Sleeuwen, 2006). However, as the global climate crisis leads to increasing temperatures and changing precipitation patterns around the globe, the frequency of extreme drought (IPCC, 2014) and in turn wildfire disturbance on these landscapes, as with much of Canada, can be expected to increase greatly within the next century (Flannigan et al., 2013). With this expected rise in wildfire risk, it is important to know and understand how wildfire impacts these landscapes in order to inform adaptive management techniques, landscape restoration, and better our understanding of the potential ecosystem responses to increased wildfire on the landscape. The aim of this thesis is to develop a simple hydrological model to examine the fill-and-spill hydrological dynamics in rock barrens wetlands and to determine the potential impacts on these dynamics due to wildfire.

Ontario's Rock Barrens Landscape

The Canadian Shield covers approximately one-third of Canada's land surface (Spence & Woo, 2008). The southern extent of Ontario's Precambrian shield region, particularly along the eastern shore of Georgian Bay, consists of exposed granite bedrock outcrops which make up Ontario's rock barrens landscape (Figure 1; Catling & Brownell, 1999). This landscape consists of bedrock ridges (Figure 2a) which have lichen- and moss-covered thin soil deposits (Figure 2b) (Hudson et al., 2020), and valleys which support bog and poor fen peatlands (Figure 2c), small mixedwood forests (Figure 2d), and lakes and ponds often formed by beaver dams (Figure 2e). Due to the impermeable nature of the granite bedrock, depressions on the landscape store water and are capable of supporting ephemeral and perennial wetlands which are isolated from regional groundwater and support the development of peat forming species such as *Sphagnum* mosses (Catling & Brownell, 1999; Didemus, 2016). The term rock barrens in this context refers to the entire landscape, not just the exposed bedrock ridges (Figure 2).

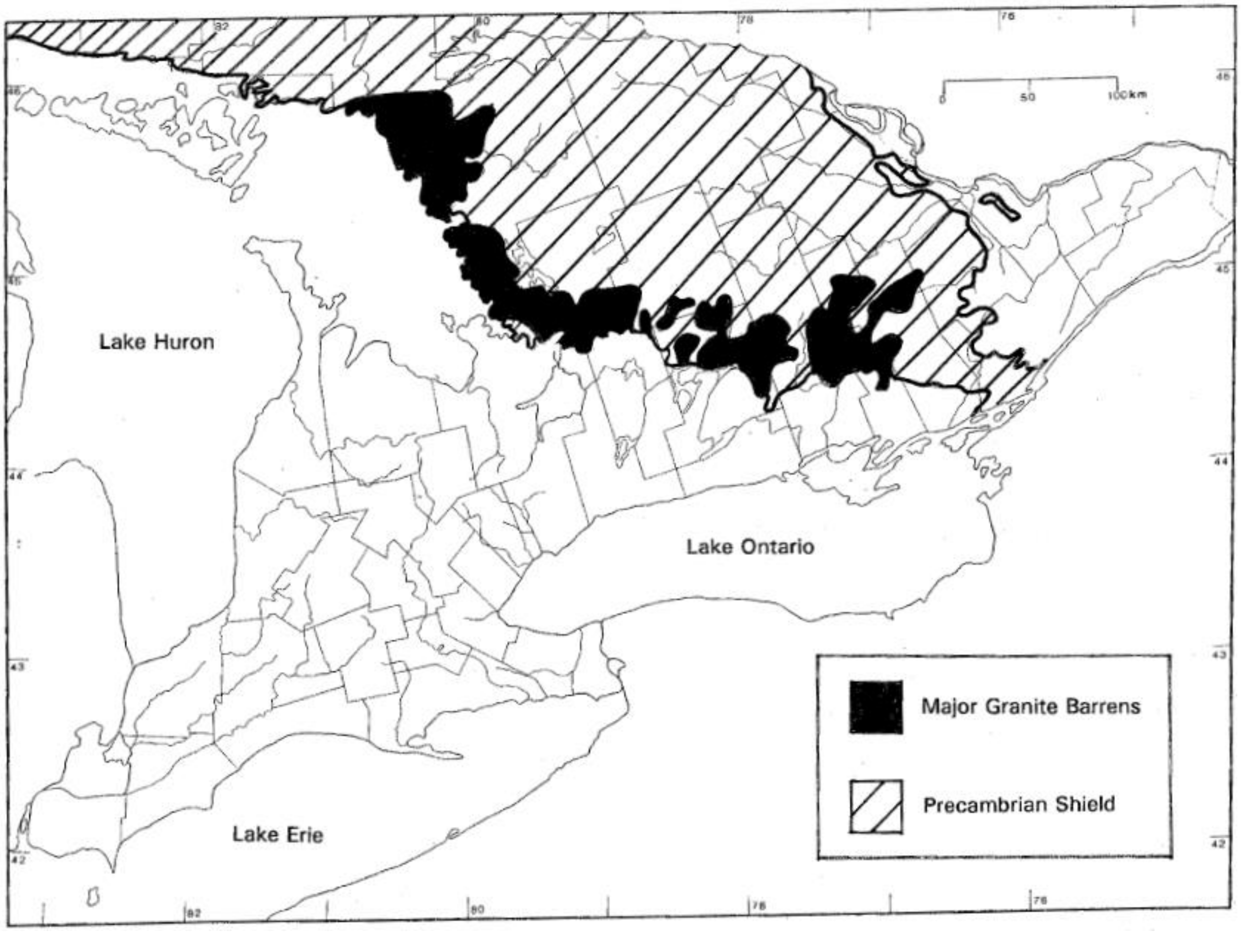

Figure 1. A map of Ontario's southern Precambrian Shield (lined area) with the rock barrens landscapes filled in solid black (from Catling and Brownell, 1999).

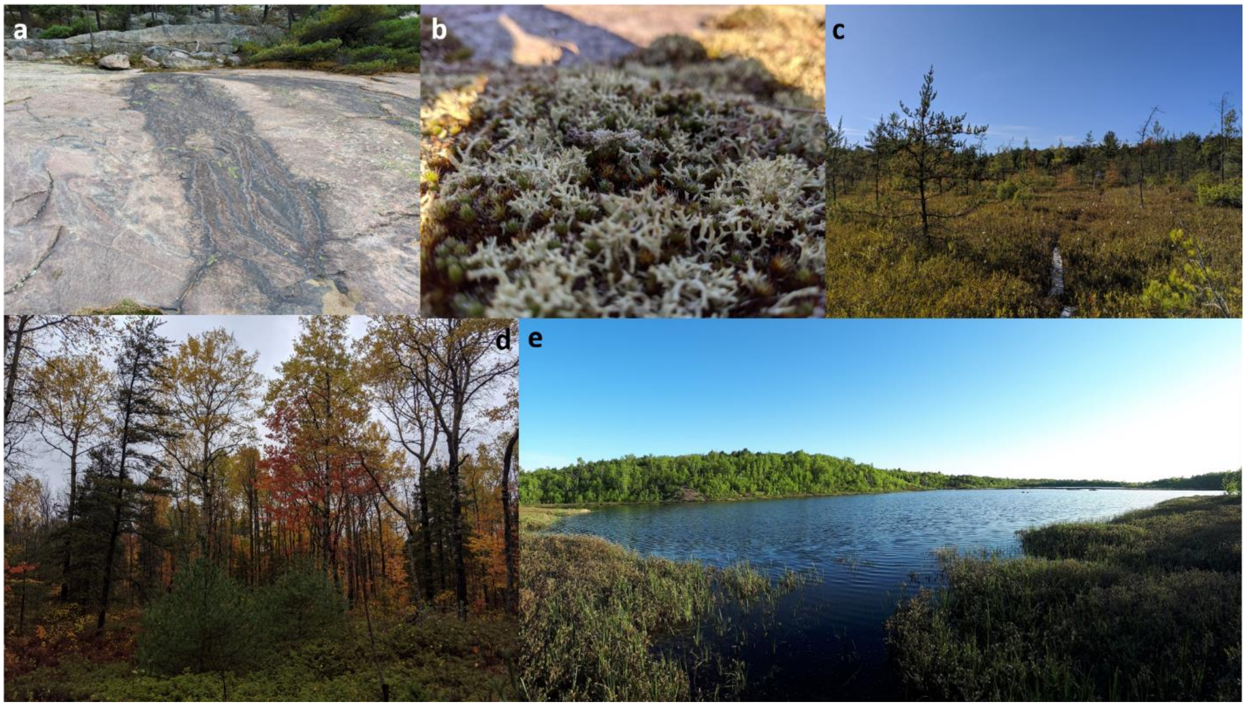

Figure 2. Typical landscape features of the rock barrens. (a) exposed granite bedrock ridges, (b) thin moss- and lichen-covered soil deposits, (c) peat-filled wetlands, (d) forested valleys and hillslopes, (e) small lakes and ponds formed in valley bottoms.

Hydrological Connectivity and the Hydrology of Rock Barrens Watersheds

Hydrological connectivity is a term that has been adopted from ecology by hydrologists as a way of describing the movement of water throughout a landscape (*e.g.*, Ali et al., 2018; Bracken & Croke, 2007). Within ecology, connectivity is used to describe the movement of organisms between various elements of a landscape (Taylor et al., 1993). Ecological connectivity, therefore, describes a landscape's ability to facilitate the movement of a species between different habitat locations and the connection between different populations on the landscape (Bracken & Croke, 2007; Taylor et al., 1993). The term's adaptation into hydrology to describe a landscape's ability to facilitate the movement of water is attractive to a variety of hydrological subdisciplines because it allows for the incorporation of various landscape types and scales as well as the addition of water facilitated transport of sediment, biological, and chemical elements throughout a landscape (Bracken & Croke, 2007). Although there is no consensus on a single definition of hydrological connectivity, recent literature has sought to provide answers to this problem in order to allow the term to become a more accepted notion in hydrology (Ali et al., 2018; Bracken & Croke, 2007; Pringle, 2001, 2003). A reasonably simple definition is provided by Pringle, (2001) which states that hydrological connectivity is the "water-mediated transfer of matter, energy, and/or organisms within or between elements of the hydrologic cycle" (p. 981). Ali et al. (2018) provide a more rigorous definition and state that hydrological connectivity is, "the occurrence of water and/or material transmission between a source A and a receptor B when the magnitude of water and/or material leaving A is larger than the magnitude of water and/or material losses that occur along the flow path from A to B" (p. 638). These definitions of hydrological connectivity show that the concept can be used in a wide variety of circumstances and at various scales (i.e., plot, hillslope, and watershed) and incorporates not just the movement of water, but also the water mediated movement of other materials, such as sediment, nutrients, and biological elements, around the landscape (Ali et al., 2018; Pringle, 2001).

As mentioned earlier, HRUs are elements distributed on the landscape which have a similar climate and pedological-topographical-geological setting which controls their response to water inputs (Flügel, 1995). Other terms have been used alongside HRU in the literature such as "hydrologically similar surfaces" which are areas of a watershed with similar response to rainfall (Kirkby et al., 2002) or "hydrological elements" which are described by Spence & Woo (2006) as elements on the landscape which, "exhibit distinct hydrological behaviour that is reflected in (their) response to snowmelt and rainfall events" (p. 150) and can be determined by differences in topography, soils, and vegetation. These terms all describe how different parts of a landscape perform different hydrological functions in response to water inputs and can be applied at different scales on the landscape as can the concept of hydrological connectivity (Bracken & Croke, 2007). Spence & Woo (2006) describe the three key functions of hydrological elements as: water storage, runoff contribution, and water transmission from and to adjacent hydrological elements. Hereafter elements on the landscape which exhibit distinct hydrological function are referred to as HRUs given the term's wide use within the literature. The functional response of an HRU to water inputs (*i.e.*, precipitation or run-in from upstream elements) is controlled primarily by the current storage deficit (*i.e.*, antecedent moisture conditions and WT position) and its thresholds to runoff generation (*i.e.*, the elevation of a sill (the spilling water level) and soil hydrophysical properties; Spence & Woo, 2003). Determining the HRUs within a watershed and their specific response to precipitation and run-in inputs is key in determining the hydrological connectivity and function of a watershed and the potential hydrological, and thus ecological, impacts that disturbance, such as wildfire will have on the landscape.

Hydrological Connectivity in Rock Barrens Landscapes

HRUs can be determined at a variety of spatial scales depending on the functional scale of the research questions in mind and the nature of the landscape in question. At a broader scale the rock barrens landscape can be divided into relatively large watersheds which feed into permanent streams, ponds, and lakes. Within these larger watersheds, individual sub-watersheds for each bedrock depression can be delineated. These bedrock depressions and their watersheds then act as HRUs within the larger watersheds, as the depression acts as a primary control on the hydrological connectivity of its sub-watershed to the larger watershed. Each depression watershed HRU can then be further sub-divided into smaller scale sub-HRUs which include exposed bedrock, moss-and lichen-covered thin soil deposits, small forested patches, and the depression itself. The bedrock ridges, which are characteristic of the rock barrens landscape, are found at topographic highs within their local landscapes and therefore these individual depression watershed HRUs act as headwaters for downstream lakes and rivers. It is important to note that larger depressions (likely supporting peatlands) will often have other smaller depressions (potentially supporting ephemeral wetlands) within their own watersheds leading to a dynamic upland contributing area with smaller depressions acting as controls on the hydrological connectivity of the larger depression's watershed. This sub-division of the rock barrens landscape allows one to study both the landscape wide hydrological dynamics and connectivity, as well as the hydrological dynamics and connectivity of individual depression watersheds.

Hydrological connectivity is used across hydrological studies that include both surface and subsurface water flows. Within rock barrens landscapes, wetland-groundwater connectivity is generally considered a non-existent or negligible aspect of the water balance, due to the relatively impermeable underlying bedrock (Catling & Brownell, 1999; Didemus, 2016; Spence & Woo, 2002; Vanschoenwinkel et al., 2009). The inflow of water into peat-filled bedrock depressions is therefore a combination of precipitation, Hortonian overland flow along exposed upland bedrock, and in some more complex systems through thin soil deposits directly adjacent to depressions (Allan & Roulet, 1994; Branfireun & Roulet, 1998; Spence & Woo, 2006). Further, when water levels reside below a depression's sill the flux of water leaving that depression is solely through evapotranspiration (ET), and only when water levels rise above the sill does discharge occur (Phillips et al., 2011; Spence, 2000). Depressions are thus hydrologically connected to their upland watershed area only when there is water flowing in along the bedrock and are only hydrologically connected to the area downstream when outflow is occurring at the sill. Bedrock depressions therefore provide a regulatory function on the connectivity of their entire watershed to downstream HRUs (Spence & Woo, 2002). During dry periods potentially large areas of the landscape may be disconnected from providing water downstream as depressions must overcome storage deficits before they become connected downstream (Spence, 2000). However, during wet periods only a small input of precipitation can cause large areas of a watershed to become connected again. This is more commonly referred as “fill-and-spill” (Spence & Woo, 2003). Thus, these dynamics in hydrological connectivity on the landscape have large implications for the movement and supply of water throughout a watershed, and any impacts, such as wildfire, to the key factors determining these dynamics will have landscape wide implications. By modelling the water balance and hydrological connectivity of ephemeral wetlands and the impacts of wildfire to these systems we can better predict the changes in connectivity and better understand the overall landscape hydrological response to disturbance.

Depression Storage

As mentioned above a key aspect in determining an HRUs response to hydrological inputs is its thresholds to discharge or spilling (Spence & Woo, 2003). In rock barrens depressions this is determined by the total storage capacity of the depression. Storage capacity is simply the maximum amount of water that can be stored within the depression and is determined by the volume and porosity of the soil within and the total volume of the depression itself. The depression volume is determined by the surface area of the depression at the elevation of the sill, the depth of the depression relative to the sill, and the shape of the profile of the depression, similar to prairie potholes studied by Hayashi & van der Kamp (2000). The shape of the profile of the depression determines depth-area-volume relationships which determine the behaviour of the WT as it changes with depth (Brooks & Hayashi, 2002). The profiles of depressions can often be complex, but overall, depression area decreases with depth. Previous work has determined depth-area-volume relationships and parameters to represent generalized shape profiles of depressional wetlands. For example, for prairie potholes in Saskatchewan, Hayashi & van der Kamp (2000) developed simple equations to represent the surface area of the water surface and the volume of water within a wetland for a given WT height and determined a shape coefficient which can be used to describe the shape of depression profiles. This methodology has a potential use in rock barrens for describing the WT, storage, and hydrological connectivity dynamics of depressional wetlands.

Hydrological Modelling in Depressional Systems

The "fill-and-spill" model of runoff generation, which has been used by many researchers to describe the hydrological connectivity of depressional systems (*e.g.*, Evenson et al., 2018a; Leibowitz et al., 2016; Spence, 2007; Spence & Woo, 2003; Tromp-van Meerveld & McDonnell, 2006), explains the mechanisms controlling hydrological connectivity of rock barrens bedrock depressions. The fill-and-spill concept can be used to conceptualize and parameterize numerical models of the patterns of hydrological connectivity between various HRUs within watersheds that are dominated by depressional wetlands, such as those in the rock barrens landscape.

More complex models have been developed for ephemeral wetland systems in which groundwater interactions need to be accounted for (*e.g.*, Pyke, 2004), however the relatively simple water balances of rock barrens depressions lend themselves to simple water balance models which can simulate the storage, WT, and hydrological connectivity dynamics of these systems. Due to the impermeable bedrock underlying these depressions the use of "bucket" models and the fill-and-spill conceptual model allow for relatively few inputs and outputs of water from storage in the depressions, with precipitation (P) and run-in (Q_{in}) representing additions to storage, and evapotranspiration (ET) and discharge (Q_{out}) being the only removals of water. E.g.:

$$\Delta S = P + Q_{in} - ET - Q_{out} \quad \text{[Q.I-1]}$$

Similar modelling approaches have been used in comparable systems such as the temporary rock pools of southern Africa (Hulsmans et al., 2008; Tuytens et al., 2014; Vanschoenwinkel et al., 2009). These ephemeral aquatic ecosystems are situated in small, straight-sided depressions or holes embedded in various impermeable bedrock. Although they are relatively smaller compared to some rock barrens depressions (depths ranging from 0.04 – 0.38 m and areas of 0.4 – 66 m^2; Hulsmans et al., 2008; Vanschoenwinkel et al., 2009) and exist in an arid climate where annual potential evapotranspiration (PET) is much greater than annual precipitation, they provide an excellent example of the implementation of simple bucket models as a tool to reconstruct historical storage dynamics (Vanschoenwinkel et al., 2009) or predict the impacts of climate change on ecosystem function (Tuytens et al., 2014). These models only require simple inputs of measured precipitation and ET, along with easily measured depression characteristics. In addition to being able to accurately reconstruct water levels within pools, one model was able to accurately match both discharge volume and hydrological connections observed between adjacent pools (Tuytens et al., 2014). A similar approach to modelling the hydrological dynamics and connectivity of rock barrens depressional wetlands would be a useful tool in assessing the impact of disturbances, such as wildfire, on wetland hydrology.

Furthermore, and as mentioned earlier, depression HRUs are often found clustered and nested within watersheds in landscapes and a spatial component of hydrological connectivity on a landscape scale can also be modelled, incorporating multiple depressions and their interactions.

For example, Evenson et al. (2018b) used the fill-and-spill concept to model surface and subsurface water flow using the SWAT-DSF model in the Greensboro watershed (a watershed in the Delmarva peninsula of Maryland dominated by depressional wetland HRUs) using high resolution spatial data of more than 1700 depression HRUs within the watershed and successfully replicated streamflow and wetland inundation patterns. This modelling approach would likely be suitable and applicable within Ontario's rock barrens landscape, which is similarly dominated by depression HRUs, by adapting a "simple" bucket model to incorporate depth-area-volume relationships and incorporating them with landscape scale spatial data. This application would be applicable both in the modelling of impacts such as wildfire and land use change as well as potentially predicting which parts of the landscape may be most vulnerable to disturbance as these impacts are often highly spatially variable and are predicted to intensify in the future (Flannigan et al., 2013; Niemi et al., 2007; Walton & Willeneuve, 1999).

Hydrological Response to Wildfire: Watersheds

Wildfire in northern regions is increasing in frequency and areal extent as anthropogenic climate change and increased land use changes are leading to the drying and build up of fuels (Flannigan et al., 2016; Flannigan & Wagner, 1991; Wotton et al., 2017). A significant increase in the areal extent of wildfire impacts has occurred in recent years (Hanes et al., 2019), and these changes to wildfire regimes are predicted to continue across Canada where some regions may see an increase of 3 to 4-fold in annual area burned in the next century when compared to the latter half of the twentieth century (Flannigan et al., 2005).

Wildfire impacts on the hydrological and ecosystem services of a landscape can persist long after the fire has been extinguished (Robinne et al., 2020). The removal of vegetation, litter, and organic soils through combustion can lead to increased surface runoff (*e.g.*, Benavides-Solorio & MacDonald, 2001; Larsen et al., 2009; Silins et al., 2009; Wilson et al., 2018). Further, the formation of hydrophobic soils following wildfire decreases soil infiltration rates and increases the occurrence of Hortonian overland flow (DeBano, 2000; Shakesby et al., 2000). Increased runoff following wildfire can enhance soil erosion as the soils are no longer protected by surface cover and vegetation (Larsen et al., 2009). The increased runoff and sediment transport are often associated with increases in nutrient loading into water bodies, contaminating aquatic ecosystems and human water supplies (Bladon et al., 2014). Following a severe wildfire within Canada's Rocky Mountains, Silins et al. (2009) found that over a 4-year period following disturbance impacted areas showed higher stream flows as well as 2-times more total suspended solids in stream effluent during base flow, 7-times more during snowmelt, and 11-times more during storm events when compared to a similar nearby unimpacted watershed. Associated increases in nutrient transport were found to persist for several years following the initial impacts (Allin et al., 2012; Bladon et al., 2008; Silins et al., 2014). The removal of the tree canopy was also associated with increased snowpack depth by approximately 62% and increased net precipitation by approximately 58% during May-September due to reduced canopy interception loss (Burles & Boon, 2011). As these impacts persist on landscapes following wildfire it is imperative to better understand the effects on landscape hydrological connectivity and subsequent impacts to ecosystem services.

Hydrological Response to Wildfire: Peatlands

The high organic content of peat provides a large amount of fuel available for smouldering combustion (Frandsen, 1987); however, once the peat surface has been ignited the extent to which the combustion reaction propagates is highly variable and the peat burn severity, or depth of burn

(DOB), can range from minimal amounts (Shetler et al., 2008) to depths up to or greater than 1 m (Lukenbach et al., 2015; Wilkinson et al., 2018). The vulnerability of a peatland to deep burning is highly associated with the factors which lead to the ability for surface moss to maintain a connection to the WT, even under high moisture deficits (Dixon et al., 2017; Hokanson et al., 2016; Lukenbach et al., 2015; Wilkinson et al., 2019). This variability in peat smouldering can make the impacts of wildfire on a peat-dominated system hard to predict as many of the impacts are dependent on peat burn severity which is inherently related to the hydrological dynamics of the system.

Peatlands have autogenic ecohydrological feedbacks which often protect their ecohydrological functions from disturbance such as wildfire (Waddington et al., 2015) and changes in peatland water balance following wildfire, through reductions in ET that protect the anaerobic conditions required for prolonged carbon storage in peat (Kettridge et al., 2014, 2017). However, high peat burn severity puts such feedbacks at risk of breaking down and can lead to increases in peatland drying following wildfire (Kettridge et al., 2019; Wilkinson et al., 2020b) which can alter the recovery trajectory of peatlands following a disturbance (Lukenbach et al., 2016). The extent to which these impacts will be observed within a unique landscape such as Ontario's rock barrens is unclear, however, the frequency of shallower peat depths within this landscape and their tendency to lose the presence of a WT during dry summers (Didemus, 2016; Moore et al., 2021) would suggest that surface peat loses its connection to the WT leaving it at risk to high peat burn severity during a wildfire (Dixon et al., 2017; Hokanson et al., 2016). In fact, Wilkinson et al. (2020a) found that pre-fire peat depth had a significant control on the DOB in the rock barrens, with peat deposits less than ~0.7 m in pre-fire depth showing substantial DOBs, where-as deposits greater than this threshold experienced relatively small, or in many cases zero

DOB. This would suggest that the greatest direct impacts of wildfire disturbance will be seen in the small ephemeral wetlands, however larger peatlands are likely still impacted by the changes in hydrological connectivity within their watersheds.

With peat properties within a depression being a key factor in determining the storage capacity and thus hydrological connectivity to the downstream landscape, the significant removal of peat from these shallow peat systems may result in an increase in storage capacity and thresholds to discharge, potentially resulting in significant changes to the landscape scale hydrological connectivity.

Wildfire in Ontario's Rock Barrens Landscape

Wildfire in Ontario has only been officially documented for a relatively short period of time (approximately 100 years) however much effort has been made to reconstruct historical fire areas through historical records and tree scar analysis (Alexander, 1980). There are also historical records of human use of wildfire in Ontario, both traditional burning (Shkode) by First Nations communities and for land clearing by European settlers (Alexander, 1980). Although fire return interval estimates for Ontario are subject to inaccuracy, within most of the Northern Ontario forest region the fire return interval is estimated to be around 500 years (Alexander, 1980). The rock barrens landscape is not a part of the regions included in Alexander (1980), but the heavy presence of Jack Pine (*Pinus banksiana*), with its serotinous cones, and other conifers on the landscape indicates that wildfire is an influencing factor in the rock barrens landscape ecosystems (Greene & Johnson, 1999). Estimates of the basal age of the thin organic soil deposits within the rock barrens show their age to be > 700 years (cal BP; Waddington, unpublished data) and thus indicates that a high impact disturbance resulting in the complete removal of organic soil has not occurred on that part of the landscape for at least 700 years. It is possible that lower intensity fires have occurred on the rock barrens in the intermittent time period which may have removed surface vegetation, but total organic soil loss within thin soil deposits due to wildfire is not a common occurrence.

The >11,000 ha (Parry Sound #33) fire which occurred in 2018 was intense enough to remove much of the thin soil deposits present on the bedrock outcrops, most likely through both combustion and increased post-fire erosion and is considered an unprecedented fire for the region (Markle et al., 2020). The slow growing nature of these thin soil deposits (Hudson et al., 2020; Shure & Ragsdale, 1977) indicates that their recovery will take a long time and restoration efforts may be necessary in order to help recover the critical habitat which species at risk use on the landscape (Markle et al., 2020). The impacts of wildfire on landscapes such as Ontario's rock barrens have not previously been studied and with increasing wildfire risk predicted for the future, the importance of this landscape for at-risk reptile species, the expansion of human settlements into the area, and the importance of hydrologic ecosystem services provided by the rock barrens, further understanding of the impacts of wildfire on this landscape will be imperative for future wildfire and ecosystem management.

Objectives

The objectives of this research are to (1) develop and parameterize a water balance model for rock barrens depressions (RHO; Rock-barrens Hydrology with Organics) to model fill-and-spill WT dynamics in the snow-free season, (2) use RHO to estimate the potential impacts of fire on the hydrological connectivity of ephemeral wetlands associated with combined changes to run-in and DOB, and (3) assess the relative contributions of changes to run-in and DOB on hydrological connectivity separately. Objective 1 is examined through detailed field surveys of ephemeral depressional wetlands in Ontario's rock barrens landscape. Depression characteristics, such as depth-area-volume relationships, are obtained and used to build models of individual depressions. Values for unknown parameters are obtained through a calibration and validation process and continuous WT data from each wetland is used to assess the model's ability to accurately predict WT, and in turn fill-and-spill dynamics, using measured precipitation and PET data. Objectives 2 and 3 are examined through various scenario tests and sensitivity analyses where changes in a connectedness index and other modelled water balance outputs are assessed with respect to changes in parameter values representing run-in and DOB.

CHAPTER 2: METHODS

Water Balance Model

The Rock-barrens Hydrology with Organics model (RHO) is a water balance model developed for simulating the storage dynamics of depressional wetlands. RHO calculates the water balance, accounting for inputs through precipitation (P) and run-in from its upslope watershed area (Q_{in}), and outputs through evapotranspiration (ET) and discharge (Q_{out}). RHO is differentiated from traditional "bucket" models as it accounts for two key features impacting storage capacity and storage dynamics in peat-filled depressional wetlands: the morphometry of the depression and the depth-dependent peat hydrophysical properties – particularly specific yield (Sy). RHO accounts for depression morphometry through depth-area-volume relationships (*e.g.,* Brooks & Hayashi, 2002; see below), and the Sy-depth relationship through the discretized layering of peat (or sediment) within the modelled depression. All modelling and data processing for this study were conducted in MATLAB R2020a or later (MATLAB, 2020).

Water Balance: Inputs

Water is added to storage in the modelled depression through two mechanisms: (1) P directly falling on the surface of the depression and (2) P falling within the upslope watershed area and reaching the depression through overland flow (Q_{in}). P is input as a depth and then calculated as a volume of water added to storage by multiplying by the surface area of the depression (A_{max}).

Q_{in} is calculated as:

$$Q_{in} = P * A_c * r \quad \text{[Eq. 1]}$$

where Q_{in} is the volume of water added to the depression storage through run-in, A_c is the area of the upslope watershed, and r is the run-off ratio of the watershed. r is calculated as a function of a watershed storage term (WSS) where:

$$r = \left(\frac{WSS}{WSS_{max}}\right)^k * (r_{max} - r_{min}) + r_{min} \quad \text{[Eq. 2]}$$

such that $r = r_{min}$ when WSS is zero, and r_{max} when $WSS = WSS_{max}$, the maximum watershed storage, with k describing the shape of this relationship. This relationship was developed based off research by Oswald et al. (2011), where they showed the impact of antecedent moisture conditions on HRU runoff in a Boreal Shield watershed. WSS is calculated daily as the previous day's WSS plus that day's P minus PET:

$$WSS_t = WSS_{t-1} + P_{t-1} - PET_{t-1} \quad \text{[Eq. 3]}$$

However, WSS cannot be negative and cannot exceed WSS_{max}.

Water Balance: Outputs

Water is removed from storage through two processes: (1) ET and (2) depression discharge (Q_{out}). Potential evapotranspiration (PET), like P, can be input as measured values which are then used to calculate storage loss through ET using the following equation:

$$ET = \begin{cases} PET * A_{peat} * E_{lim} & h_{WT} \leq d_{peat} \\ PET * A_{WT} & h_{WT} > d_{peat} \end{cases} \quad \text{[Eq. 4]}$$

where, ET is the volume of water lost from storage through the process of ET, PET is the maximum depth of water per unit area that can be lost through ET, A_{peat} is the area of the peat surface, A_{WT} is the surface area of the WT at its current height (h_{WT}) above the depression base, and E_{lim} is a limitation factor calculated as follows:

$$E_{lim} = \begin{cases} 1 & h_{WT} \geq h_{thresh} \\ \frac{h_{WT} - h_{off}}{h_{thresh} - h_{off}} & h_{off} < h_{WT} < h_{thresh} \\ 0 & h_{WT} \leq h_{off} \end{cases} \quad \text{[Eq. 5]}$$

where h_{WT} is the current height of the WT above the lowest point in the depression, h_{off} is the height above the lowest point in the depression where *ET* stops, and h_{thresh} is the height above the lowest point in the depression such that *ET* is no longer limited.

This *ET* limitation is based on observations in other peatland ecosystems where at a certain WT depth *ET* starts to decouple from *PET*. Here unsaturated hydraulic conductivity decreases several orders of magnitude and cannot meet evaporative demand and *ET* slows. Eventually the WT reaches a lower depth where *ET* is ~0 due to a lack of hydrological connection between the WT and the peat surface (Joon Kim & Verma, 1996; Waddington et al., 2015). Note that in these shallow ephemeral systems the E_{lim} function is not used as the depth of the wetlands are less than h_{off}.

Outflow occurs when the WT is above the elevation of the depression sill, when $h_{WT} < h_0$, $Q_{out} = 0$. However, when $h_{WT} > h_0$, Q_{out} is calculated using the Manning equation as follows:

$$Q_{out} = \left(\frac{86400\left(\frac{s}{day}\right)}{n}\right) * A_{out} * R_{out}^{\frac{2}{3}} * \sqrt{S} \quad \text{[Eq. 6]}$$

where n is the Manning resistance coefficient (in s m$^{-1/3}$), S is the slope of the outflow channel, R_{out} is the hydraulic radius of the outflow (in m) given by:

$$R_{out} = \frac{A_{out}}{P_{out}} \quad \text{[Eq. 7]}$$

where A_{out} is the cross-sectional area of the outflow (in m^2) given by:

$$A_{out} = W_{outlet} * (h_{WT} - h_0) \quad \text{[Eq. 8]}$$

where W_{outlet} is the width of the outflow (in m) and $h_{WT} - h_0$ is the height of the WT above the sill (in m), and P_{out} is the wetted perimeter (in m) given by:

$$P_{out} = W_{outlet} + 2 * (h_{WT} - h_0) \quad \text{[Eq. 9]}$$

Thus, Q_{out} is controlled by the prescribed values for W_{outlet}, S, n, and the height of the WT above the sill which changes with changes in storage. Due to limitations in accessing the field at the time of the study, field data was not sufficient to properly parameterize the Manning equation and thus values expressed later are functional, but do not necessarily correspond to any specific measurable feature that would be seen in the field. Thus, the Manning equation in this context has been converted to act as an empirical model of depression outflow based on h_{WT} by using one parameter (W_{outlet}) as a representation of the site's ability to shed water and holding all other parameters constant across all sites.

Water Balance: Storage

A change in storage within the depression is represented by a change in the WT elevation, with additions causing the WT to rise and losses causing the WT to drop. The daily change in storage is the net difference between daily additions and losses. Both the decrease in peat *Sy* with depth and the depth-area-volume relationship of the depression means that the change in WT position associated with a change in storage is not the same for different initial WT positions, but rather the change in WT position for a given change in storage is dependent on the position of the WT relative to the lowest point in the depression and the surface of the peat profile. Deeper in the peat profile *Sy* is low and closer to the lowest point in the depression the associated depression area is also much lower, thus a given change in storage will result in a relatively large change in the WT position. In contrast, when the WT is closer to the peat surface and closer to the elevation of the sill (h_0), *Sy* is high and the associated depression area is also high, thus the change in the WT position associated with a change in storage is comparatively less than in the former scenario. The ephemeral nature of the depressions in this study indicate that the WT can be present at all positions available within the depression thus representing the need for a detailed understanding of the characteristics of both the *Sy* relationship with depth and the depth-area-volume relationships or depression morphometry to accurately model their hydrological dynamics.

Specific Yield

Peat cores up to a depth of 0.45 m were collected from unburned peat deposits within the research area, divided into 0.05 m increments, and were analyzed for moisture retention on pressure plates (see Didemus, 2016). *Sy* was calculated as the change in volumetric water content between saturation (or the total porosity of the peat) and 10 mb tension (the lowest measured tension in the analysis) and represents the effective amount of water readily available to be removed with a change in WT position. An exponential of the form:

$$Sy = Sy_{max} * e^{-Sy_{slope} * x} \quad \text{[Eq. 10]}$$

was fit to the data where Sy_{max} and Sy_{slope} are fit parameters and x is the effective depth below the peat surface. This equation, with Sy_{max} = 0.855 and Sy_{slope} = 6.19, represents an average peat profile for peat filled depressions within the study region and is used to constrain the calibration of these parameters in RHO to calculate the *Sy* within each discretized layer of the modelled depression. For use in RHO, x can be calculated as the total depth of peat (d_{peat}) minus the height above the depression base, h, which allows for calculation of *Sy* in relation to the elevation above the deepest point in the depression.

Depth-Area-Volume

As described below, the *p-shape* parameter is used to approximate the morphometry of depressions in RHO. To calculate the volume of the depression, including both peat and pore space, below a given elevation, *h*, the following equation from Brooks & Hayashi, (2002) is used:

$$V = \frac{A_{max} * h_0}{1+\frac{2}{p-shape}} \left(\frac{h}{h_0}\right)^{1+\frac{2}{p-shape}} \quad \text{[Eq. 11]}$$

The total volume of the depression can be calculated by setting $h = h_0$. To calculate the volume of each discretized layer Eq. 11 is modified as follows:

$$V_i = \frac{A_{max} * h_0}{1+\frac{2}{p-shape}} * \left[\left(\frac{h_i}{h_0}\right)^{1+\frac{2}{p-shape}} - \left(\frac{h_{i-1}}{h_0}\right)^{1+\frac{2}{p-shape}}\right] \quad \text{[Eq. 12]}$$

Where h_i is the height above the deepest point in the depression of a single layer, *i*. Equation 12 calculates the volume in the depression below h_i minus the volume in the depression below h_{i-1}. The thickness of layers can be changed, but for the purposes of this study thickness is set to 0.001 m. To calculate the volume of extractable water (or fillable pore space) the volume of each layer is multiplied by the corresponding *Sy* of that layer as calculated using Eq. 10.

$$V_{storage\ i} = V_i * (Sy_{max} * e^{-Sy_{slope}(d_{peat} - h_i)}) \quad \text{[Eq. 13]}$$

The volume of water in storage can be calculated as:

$$V_{storage} = \sum_{i=1}^{k} V_{storage\ i} \quad \text{[Eq. 14]}$$

where $k = i$ when $h_i = h_{WT}$.

An initial WT elevation is set for the first day of the simulation, and for subsequent days the previous day's calculated WT is used as h_{WT} within the above equations. As mentioned earlier, the model calculates the total change in volume in storage and the new storage for each day in the simulation. It then calculates the new WT elevation by finding the layer in which the WT would reside corresponding to the new $V_{storage}$ and records $V_{storage}$ and h_{WT} as outputs. Other outputs include P, PET, ET, Q_{in}, and Q_{out}.

$$\Delta V_{storage} = P * A_{max} + Q_{in} - ET - Q_{out} \quad \text{[Eq. 15]}$$

Table 1a. All RHO input parameters and descriptions.

RHO Input Parameters

Symbol	Parameter Name	Units	Description	Related Equations
A_c	Upslope Watershed Area	m^2	The area of the depression watershed (not including the depression itself)	Eq. 1
WSS_{max}	Maximum Watershed Storage	m	The maximum depth of storage in the watershed, when reached $r = r_{max}$	Eq. 2
r_{min}	Minimum Run-in Ratio	-	The runoff ratio when WSS = 0	Eq. 2
r_{max}	Maximum Run-in Ratio	-	The runoff ratio when WSS = WSS_{max}	Eq. 2
k	WSS/Run-in Ratio relation shape	-	The shape parameter describing the shape of the WSS/run-in ratio relationship	Eq. 2
A_{max}	Maximum Area	m^2	The area of the depression at the elevation of the sill	Eq. 11, 12, 15, 16
p (or p-shape)	p-shape parameter	-	The parameter used in depth-area-volume relationships to describe the morphometry of the depression	Eq. 11, 12, 16
h_0	Maximum Depth	m	The change in elevation from the lowest point in the depression to the elevation of the depression sill	Eq. 8, 9, 11, 12, 16
d_{peat}	Peat Depth	m	The depth of peat within the depression at the deepest location	Eq. 4, 13
h_{thresh}	ET limiting WT elevation	m	The elevation of the WT such that when $h_{WT} < h_{thresh}$ ET is limited	Eq. 5
h_{off}	ET shutoff WT elevation	m	The elevation of the WT such that when $h_{WT} < h_{off}$ ET is set to 0	Eq. 5
Sy_{max}	Sy relation with depth parameter 1	-	A parameter derived from fitting Eq. 11 to Sy with depth data	Eq. 10
Sy_{slope}	Sy relation with depth parameter 2	-	A parameter derived from fitting Eq. 11 to Sy with depth data	Eq. 10
W_{outlet}	Outflow Width	m	The theoretical width of the depression outflow channel	Eq. 8, 9
S	Outflow Slope	-	The theoretical slope of the depression outflow channel	Eq. 6
n	Outflow Manning Resistance	$s\ m^{-1/3}$	The Manning resistance coefficient of the depression outflow channel	Eq. 6

Table 1b. Other calculated parameters in RHO.

Other Calculated Parameters

Symbol	Parameter Name	Units	Description	Related Equations
A	Area	m^2	The area of the depression at a given elevation, h, above the deepest point	Eq. 16
h	Relative Elevation	m	A height above the deepest point in the depression	Eq. 11, 16
WSS	Watershed Storage	m	The depth of water in storage in the depression watershed.	Eq. 2, 3
r	Run-in Ratio	-	The calculated run-in ratio for a given day	Eq. 1, 2
A_{peat}	Peat surface area	m^2	The area of the peat surface	Eq. 4
A_{WT}	WT surface area	m^2	The area of the WT surface	Eq. 4
E_{lim}	ET limitation	-	The factor applied to limit ET when $h_{lim} > h_{WT} > h_{off}$	Eq. 4, 5
A_{out}	Outflow Area	m^2	The theoretical cross-sectional area of the depression outflow	Eq. 6, 7, 8
R_{out}	Outflow Radius	m	The theoretical hydrological radius of the depression outflow	Eq. 6, 7
P_{out}	Wetted Perimeter	m	The wetted perimeter used in the Manning Equation	Eq. 7, 9
Sy	Specific yield	$m^3\ m^{-3}$	The effective pore space available for storage within the peat matrix	Eq. 10
x	Depth in peat profile	m	The depth from the surface within the peat profile	Eq. 10
V	Depression volume	m^3	The volume of the depression below a given elevation	Eq. 11
V_i	Layer volume	m^3	The volume of an individual discretized layer, i	Eq. 12
h_i	Layer height	m	The height above the deepest point in the depression of an individual discretized layer, i	Eq. 12
$V_{storage\ i}$	Layer storage volume	m^3	The volume of storage within a given layer, i	Eq. 13, 14

Table 1c. RHO primary water balance and model outputs.

RHO Primary Water Balance Output

Symbol	Parameter Name	Units	Description	Related Equations
P	Precipitation	m	The depth of water which falls as precipitation	Eq. 1, 3, 15
Q_{in}	Run-in	m^3	The volume of water which enters the depression through overland flow from its watershed area	Eq. 1, 15
PET	Potential Evapotranspiration	m	The maximum potential depth of water which can be removed from the depression through ET	Eq. 3, 4
ET	Evapotranspiration	m^3	The volume of water which is removed through the process of evapotranspiration	Eq. 4, 15
Q_{out}	Depression discharge	m^3	The volume of water which leaves the depression through the depression outflow	Eq. 6, 15
h_{WT}	WT elevation	m	The elevation of the WT relative to the deepest point in the depression	Eq. 4, 5, 8, 9
$V_{storage}$	Storage	m^3	The volume of water in storage in the depression	Eq. 14, 15

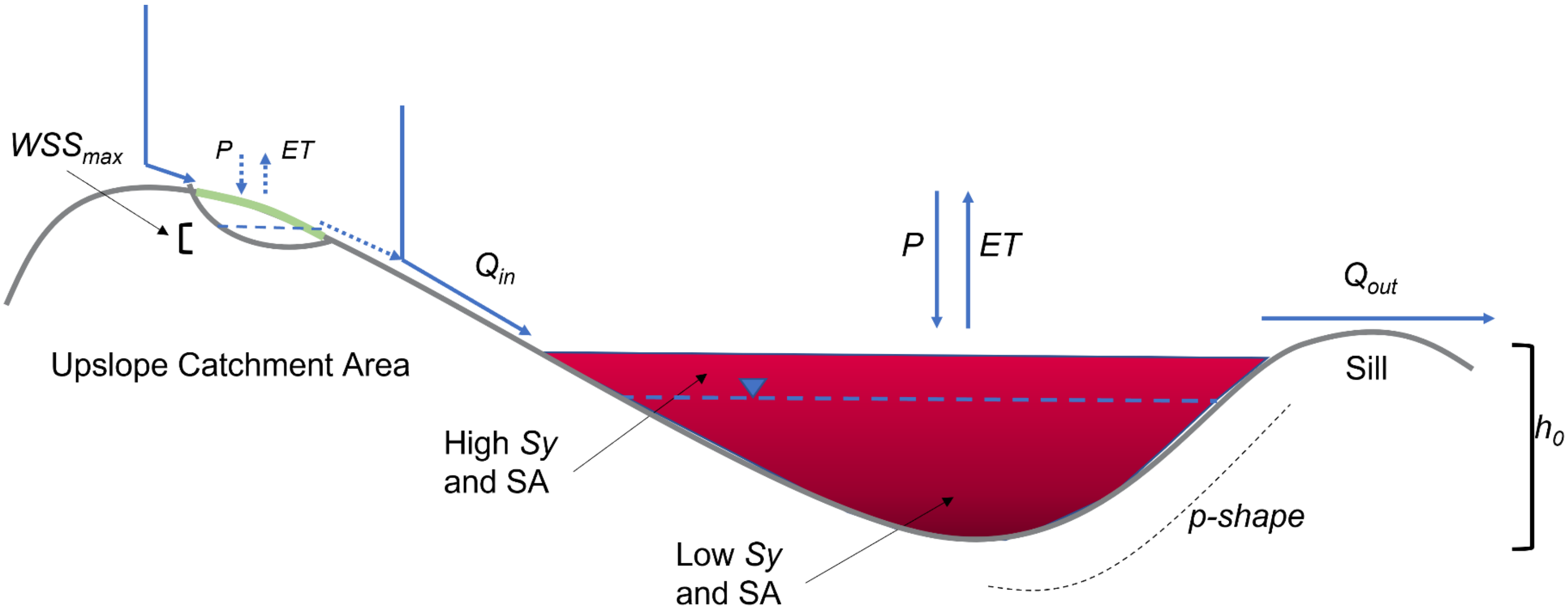

Figure 3. Conceptual diagram of RHO inputs and outputs and key parameters.

Field

Study Sites

Six ephemeral wetlands were selected for this study; three located within an unburned portion of the rock barrens landscape just north of Parry Sound, ON (sites A-C); and three within the southern footprint of the Parry Sound 33 (PS33) wildfire – approximately 90 km north of the unburned site locations (sites D-F). PS33 burned over 11,000 ha of rock barrens landscape in the summer of 2018. Following the fire, Wilkinson et al. (2020a) found that peat deposits less than 0.7 m deep exhibited deeper burning and thus sites were selected to have a maximum depth less than 0.7 m. This depth also helped to ensure all sites were ephemeral wetlands. All sites are located within the Georgian Bay Biosphere Mnidoo Gamii, a UNESCO biosphere, situated within the Robinson-Huron Treaty of 1850 and the Williams Treaty of 1923, and located on Anishinaabek territory. The sites are all situated on bedrock outcrops and have upland watershed areas that contain no other major bedrock depressions. Sites A-C are a part of a long-term ecohydrological research project and were selected for their data availability and known site characteristics (i.e., depth). Sites D-F were selected in the summer and fall of 2019 and selected based on visual assessments of the size of wetlands and initial measurements of peat depth to determine if they were < 0.7 m in depth. Because of data limitations sites D-F are only used for the field survey data and are not included in the modelling analysis of this study.

Each site was instrumented with a PVC monitoring well inserted to the underlying bedrock at the deepest known location within the depression, and a water lever recorder (Solinst Levelogger, Georgetown, ON) was installed at the base of the well to monitor water level continuously (measured every 15-minutes) and data from the snow free seasons of 2017-2019 are used in this study. Barometric pressure, used for converting absolute pressure in the water level recorders to water pressure, was recorded at a central location for each group of sites, A-C, and D-F, respectively.

Model Input Meteorological Measurements

Tipping bucket rain gauges logged half-hourly precipitation at 5 locations throughout the unburned study area (~0.6 km^2) during the study period. To fill gaps in data and account for general variability in precipitation measurements the average precipitation for each half hour was taken from sites that were recording at the time, and then was converted to daily precipitation. To fill any remaining gaps in the daily precipitation data from the Environment Canada Parry Sound CCG station (Environment and Climate Change Canada, 2019) were used. Half hourly PET was calculated with the Penman equation using air temperature, relative humidity (CS-215; Campbell Scientific, Logan, Utah), wind speed (03101 Wind Sentry; RM Young, Traverse City, Michigan), and net radiation (NR-LITE2, CS) (with the assumption that ground heat flux was 10% of the net radiation) recorded using a CR1000 datalogger (CS) at a micrometeorological station located in a peatland within the unburned research area. Half hourly data was then converted to daily data. As noted, precipitation and PET data were not collected at the burned site locations (sites D-F) for a long enough period for this study and have been excluded from the modelling analysis.

Wetland Depression Morphometry Surveys

Detailed surveys were conducted at each site to determine the morphometry of the wetland depression including surface topography, depth to mineral soil or bedrock, and the bedrock sill (the lowest point in the perimeter of the depression or the depression spill point). A Leica Disto S910 laser distance meter (Hexagon - Leica Geosystems AG, Heerbrugg, Switzerland; +/- 1.0 mm accuracy in distance and -0.1/+0.2 degrees accuracy in measuring tilt) was used to measure the surface elevation relative to a set datum on a 1 x 1 m grid across the entirety of the depression. At each location, the depth of the peat to the underlying bedrock was measured using a thin rod. The relative bedrock elevation was calculated by subtracting the peat depth from the relative surface elevation. Due to visual obstructions from vegetation some points were moved ~0.5 m in one direction or were excluded from the survey. The elevation at the location of the WT well was also measured. The data were processed in ArcMAP 10.7, and a digital elevation model of the underlying bedrock was generated using the nearest neighbour method.

Area-height Relation

The *Area-height (A-h*) relation method derived from Hayashi & van der Kamp, (2000) was used to determine a shape parameter (*p-shape*) for each site. The following equation was fit to the data using the *fit* function in MATLAB:

$$A = A_{max} \left(\frac{h}{h_0}\right)^{\frac{2}{p-shape}} \quad \text{[Eq. 16]}$$

where A is the surface area at a given height, h, above the deepest point in the depression, A_{max} is the maximum surface area at the maximum height, h_0 (can also be thought of as the maximum depression depth relative to the sill), and *p-shape* is the shape parameter which determines the shape of the relationship between A and h (Hayashi & van der Kamp, 2000). The area at a given relative elevation, h, was determined as the number of grid cells within the digital elevation model that had elevations ≤ h multiplied by the grid cell size. The maximum area (A_{max}) was calculated as the number of grid cells that were ≤ the relative elevation of the depression sill (or h_0) multiplied by the grid cell size. Ten discrete, equally spaced h values and their associated areas were used to fit the *p-shape* parameter for each site.

Watershed Area

Watersheds for sites were delineated in ArcGIS Pro, using 1 x 1 m digital elevation models of the two study areas created using high resolution aerial LiDAR data (with point spacing of 0.48 and 0.36 m for the unburned and burned areas, respectively) collected between 2019 and 2020. Pour points for watersheds were set to the estimated location of the sill of each depression (or the closest point along a flow accumulation path to the sill). The upslope watershed area of the depression was then set to be the delineated watershed area minus the maximum surface area of the depression at the elevation of the sill.

Calibration

Sites A-C have measured P, PET, and WT data from 2015-2020 and were therefore chosen for calibrating and validating RHO for the snow free season. Sites D-F did not have the data necessary for this step. The calibration and validation were done as a test of the confidence in the model's ability to accurately simulate hydrological dynamics in rock barrens wetlands. Using data collected from the field surveys most input parameters were calculated and incorporated directly into the model. However, several parameters were not measurable at the time of the field surveys, specifically WSS_{max}, r_{min}, r_{max}, k, W_{outlet}, S, and n.

W_{outlet}, S, and n all have a control on the rate of Q_{out}, and as such the final parameter values used following calibration are only locally optimal and do not necessarily correspond with the true values due to model equifinality. As mentioned above, the Manning equation is adapted to act as an empirical relationship between h_{WT} and discharge, using a single parameter to control this relationship. Thus, W_{outlet} was chosen as the single parameter to represent the control on discharge in the model, with S and n being held constant, somewhat arbitrarily, at 0.25 and 0.1 s m$^{-1/3}$, respectively. The value for n is roughly based on a number of estimates of the Manning resistance coefficient (*e.g.,* Ferguson et al., 2017; Yochum, 2018). In addition to the remaining five "free" parameters Sy_{max} and Sy_{slope}, the surface Sy and the slope of the Sy/depth relationship respectively, were included in the parameter calibration to account for the potential variability of peat properties between sites that are not necessarily represented sufficiently in the generalized peat core analysis previously mentioned.

A Monte Carlo calibration procedure which resulted in an estimate of the values of all seven parameters for each of sites A-C was used. Each site was set up separately in RHO and measured P and PET data from 2017 and 2018 were input directly into the model. The model was run 20,000 times for each site with a randomly selected value within a set range, which loosely constrained parameters within realistic values (Table 2) being assigned to each of the seven previously mentioned parameters in each run, resulting in 20,000 unique parameter sets for each of the three sites. The resulting model-predicted WT for each parameter set was compared to measured WT from 2017 and 2018 from the corresponding site and a number of model performance metrics were calculated. RMSE was selected as the metric of choice and the parameter set with the lowest scoring RMSE for each site was selected as the optimum parameter set for that site.

Table 2. Parameter ranges for calibration in RHO.

Parameter	Units	Calibration Range
WSS_{max}	m	0 – 0.5
r_{min}	-	0 – 1
r_{max}	-	r_{min} – 1
k	-	0.5 – 2
W_{outlet}	m	0 – 0.1
Sy_{max}	-	0.5 – 0.9
Sy_{slope}	-	4.5 – 8.5

Due to the loss of the WT in ephemeral wetlands and the fact that the water level recorders were not placed in the absolute deepest spot in the depression some data were not included in the RMSE calculations. During the snow-free season, on days where the observed WT dropped below the water level recorder the site was considered to have lost its WT and where the associated modelled WT values were below this minimum observed WT were excluded from the analysis. This was done because it was not possible to "observe" WT behaviour below this minimum WT and thus the performance of the model could not be accurately assessed. However, on days where the modelled WT was above the minimum observed WT when the observed data indicated that the WT should be lost, or where the modelled WT is below the minimum observed WT and the observed WT data show the presence of a WT, are included in the RMSE calculation to include data where it is known that the modelled data is inaccurate. This solution was adopted because the primary concern for this modelling exercise is the WT behaviour at or near the elevation of the sill to ensure that the model can accurately capture spilling events. The exclusion of this data is reflected in figures using observed and modelled WT data.

High quality data was available for 2017 through 2019. 2017 and 2018 were selected as the calibration data set in order to capture a range of hydrological conditions. In 2017 the sites never experienced a complete loss of WT and therefore represents a particularly "wet" year, whereas 2018 was a "typical" summer (if not particularly dry summer) in which all the sites experienced WT losses (see McDonald, 2021). This was done with the intention of producing parameter sets which would be representative of processes under a full range of conditions which would be applicable in more scenarios. The selected "best" parameter sets for each site were then used in a validation run using input *P* and *PET* and compared to WT data from 2019. RMSE was calculated and used to determine the validity of the parameter values determined in the calibration.

The model is calibrated and validated for the snow-free season using data from April 1st to October 31st (DOY 91 – 304). Initial WT values for the start of each model run were selected as the WT elevation on the day before the first day of the model run (March 31st, or DOY 90).

Parameter Uncertainty

The top 1% of parameter sets (200 best performing parameter sets) from the calibration procedure for each site were used to assess the uncertainty around the calibrated parameter values. First, RMSE was plotted against the individual calibrated parameter values and due to the non-parametric nature of the data a Spearman rank correlation was performed on each comparison to reveal potential correlations between individual parameter values and model performance, where correlation coefficients range from -1, a perfect negative correlation, to 1, a perfect positive correlation.

Wildfire Impacts Modelling

To assess the effects of wildfire disturbance on the water balance and hydrologic connectivity of depressional wetlands in Ontario's rock barrens a series of scenario tests were conducted. Scenario tests were conducted at two levels, the first relating to the second research objective, comparing an unburned to a burned depression by changing impacted parameters related to run-in, r_{min} and r_{max}, and DOB, and the second relating to the third research objective by testing impacts to only run-in and impacts to only DOB. Briefly, a hypothetical depression was created in RHO using parameter values within the range of both measured and calibrated parameters (Table 3). This modelled depression was used as the basis for scenarios where all parameters were held constant, except for the parameters changed for the specific scenario being tested. To compare scenarios, a connectedness index was calculated as the number of days on which discharge occurred divided by the total number of days in the simulation. This metric enabled the examination of the impacts of fire on the fill-and-spill behaviour of ephemeral wetlands. See scenario testing and factorial scenario test sections below for more details.

Table 3. Parameter descriptions and values for the constant parameters across scenario tests and sensitivity analyses. See Chapter 1 for further details on model structure.

Parameter	Description	Units	Value
E_{max}	Maximum daily PET for the summer solstice – used in stochastic PET generation	m	0.007
E_{min}	"Minimum" daily PET, or the highest PET possible for the winter solstice – used in stochastic PET generation	m	0.0005
A_c	The area of the watershed upslope of the depression (not including the depression itself)	m^2	365
WSS_{max}	The maximum depth of storage in the watershed, when reached $r = r_{max}$	m	0.25
k	The shape parameter describing the shape of the WSS/run-in ratio relationship	-	1
A_{max}	The area of the depression at the elevation of the sill	m^2	120
p-shape	The parameter used in depth-area-volume relationships to describe the morphometry of the depression	-	0.9
h_0	The change in elevation from the lowest point in the depression to the elevation of the depression sill. The maximum depth of the depression.	m	0.6
$d_{ub\text{-}peat}$	The "pre-fire" depth of peat – assumed to equal to h_0	m	0.6
Sy_{max}	The Sy of peat at the surface, or the maximum specific yield.	-	0.82
Sy_{slope}	The slope of the curve of the Sy with depth relationship.	-	4.75
W_{outlet}	The theoretical width of the depression outflow channel	m	0.003
S	The theoretical slope of the depression outflow channel	-	0.25
n	The Manning resistance coefficient of the depression outflow channel	$s\ m^{-1/3}$	0.1

Stochastic Precipitation and Potential Evapotranspiration

To obtain a large sample size to account for variability in precipitation and PET, precipitation and PET data were generated using stochastic equations within RHO. Precipitation data was generated by assigning a precipitation depth to each day through the random selection of a value from a Weibull distribution of statistically realistic rainfall. The precipitation depth was then applied using an equation that determines the days on which precipitation occurs based on the typical fraction of days in a year with or without precipitation (see Appendix).

To generate PET data, first, a generic sinusoidal curve of the maximum possible PET for each day in the simulation was generated. This was made based on a set maximum possible PET for the winter solstice and maximum possible PET for the summer solstice (E_{min} and E_{max}, respectively) to account for the seasonality of PET. Next, the cloud cover for each day was simulated to determine the proportion of solar radiation reaching the ground by randomly selecting values from two distributions, one for days without rain and one for days with rain (as determined by the already generated precipitation data). The cloud cover distributions were made based on weather patterns from Northern Michigan which has similar climatic and weather conditions as eastern Georgian Bay. Finally, the original theoretical daily maximum PET values were multiplied by the proportion of radiation reaching the ground as determined by the cloud distributions. For the purposes of this study E_{max} and E_{min} were set to 0.007 and 0.0005 m, respectively. These values were parameterised by data previously collected at the study site. 1000 years of precipitation and PET data were generated and used for all scenario testing and stepwise sensitivity analyses for consistent comparison between scenarios. (See Appendix for equations and further information on the generation of stochastic precipitation and PET data.)

Depth of Burn and Specific Yield

In the event of a wildfire, smouldering combustion removes the top layer of live moss and peat from the peat profile, referred to as the depth of burn (DOB). DOB can range from a few centimeters (Benscoter & Wieder, 2003; Wilkinson et al., 2020a) to over 1 m deep in dry dense peat (Lukenbach et al., 2015; Wilkinson et al., 2018). This exposes peat lower in the profile which typically has a lower Sy than the peat closer to the surface. To account for this change in the peat profile the Sy profile of an unburned depression was generated and then modified such that the Sy was set equal to one for any space within the depression above the new ground surface (as determined by DOB) and below the depression sill. Other work has shown that the Sy profile of peatlands is further impacted by burning (Sherwood et al., 2013), however the extent to which this occurs in rock barrens peat is unknown, and thus the method used is a conservative estimate of the impacts of DOB on Sy.

Scenario Testing

To address objective 2 the first scenario test compared the unburned depression to a wildfire impact scenario, where r_{min} and r_{max} were increased from 0.05 and 0.7 to 0.25 and 1, respectively (Table 4). As studies on the impacts of wildfire on the hillslope hydrology of the rock barrens have not been conducted before these values were chosen to represent a worst-case scenario increase to run-in, and to be higher than the maximum values found during the calibration of RHO to unburned sites. The DOB for this scenario was set to 0.15 m (Table 4), which is a conservative estimate of the possible DOB based on the relationship between pre-fire peat depth and percent burned from Wilkinson et al. (2020a) for a depression with a maximum depth of 0.6 m pre-fire peat depth, accounting for the range of depths associate with depression morphometry.

To address objective 3 this test was sub-divided into two additional scenarios, one assessing the impact of changing DOB alone and one where only r_{min} and r_{max} were tested (Table 4). This was done to break the testing into two main impacts, direct peat combustion in the depression and impacts to the depression upslope watershed area, to better understand which impact may have the bigger effect on model output. For all scenario tests the initial WT position was set to the elevation of the sill, unless otherwise noted, to represent the typical wet conditions within ephemeral wetlands in the spring.

Table 4. Parameter values for unburned and worst-case scenario testing.

Parameter	Unburned	Fully Burned	Burned Depression	Burned Uplands
r_{min}	0.05	0.25	0.05	0.25
r_{max}	0.7	1	0.7	1
DOB (m)	0	0.15	0.15	0

Statistical Analyses

A Kolmogorov-Smirnov test was used to test the normality of the connectedness index from scenarios. In all cases the null hypothesis was rejected, finding that the data does not fit a normal distribution. A Kruskal-Wallis test was then used to test the significance of the difference between burn scenarios. For burn scenario test results data reported are median (± standard error), unless otherwise stated.

Sensitivity Analyses

A one-at-a-time (OAT) stepwise sensitivity analysis was conducted, where each “impacted” parameter was isolated and incrementally changed to see the sensitivity of the connectedness index to changes in specific parameters and to reveal any threshold behaviour within the system. The modelled depression was set up in RHO and each model run then used the same 1000 years of stochastically generated precipitation and PET data. One at a time a single impacted parameter was set at varying set points while the other two parameters were held at their original value. r_{min} was increased at steps of 0.05 starting at 0.05 up to 0.5, r_{max} was also increased at steps of 0.05 starting at 0.7 up to 1.0, and DOB was increased at increments of 0.05 m starting at 0 up to 0.6 m (representing a complete removal of peat within the depression). The connectedness index for each model run was calculated and the median and standard errors of connectedness indices for each parameter set point were used for comparisons.

Factorial Scenario Test

A factorial scenario test was conducted, where the same base depression was set up in the model and incremental changes to r_{min}, r_{max}, and DOB were applied at the same time. DOB was increased at increments of 0.01 m starting at 0 up to 0.1 m, as this is the DOB after which the model shows no significant change in connectedness as per the stepwise one-at-a-time sensitivity analysis. For each DOB three main sets of r_{min} and r_{max} scenarios were tested. First, r_{min} was increased at increments of 0.05 from 0.05 to 0.2 while r_{max} was held at 0.7. Second, r_{min} was held constant at 0.05 while r_{max} was increased at increments of 0.1 from 0.7 to 1. And finally, r_{min} and r_{max} were both increased at the same time. This created 10 unique r_{min}/r_{max} combinations, and with 11 DOB steps there are a total of 110 different burn scenario combinations. For each scenario the same 1000 years of stochastic precipitation and PET data were used. In addition to the median connectedness index as used in the above scenario tests, the median Q_{out}, median Q_{in}, and median ET as calculated by the model were also included in the factorial analysis to compare model outputs and help explain differences in the overall water balance to further explain changes to hydrologic connectivity between scenarios.

CHAPTER 3: RESULTS

Field Surveys

Maximum depression depth (relative to the depression sill) ranges between 0.38 and 0.71 m (sites E and B respectively) with a mean maximum depth of 0.53 m. Mean surface area at the elevation of the sill is 125.6 m^2 with site A having the lowest surface area at 116 m^2 and site F having the largest surface area at 150 m^2. Upslope watershed area ranges considerably with two of the six sites having watershed areas less than 200 m^2, A and D at 198 and 82 m^2, respectively. The remaining sites have upslope watershed areas greater than 250 m^2 with the largest being site B at 649 m^2, while mean watershed area is 377 m^2 (Table 5; Figure 4).

P-shape parameters using the A-h method range between 0.61 and 1.66 (sites B and D respectively) and have a mean of 1.16 (Figure 5). Although wildfire would have no impact on the bedrock morphometry, it is interesting to note that sites in the unburned study area (A-C) all have *p-shape* values ≤ 1, or exhibiting a convex cross section, while sites in the burn study area (D-F) all have *p-shape* values ≥ 1.3, or exhibit a concave cross section (Figure 5; Table 5).

Table 5. Parameter values measured through field surveys and geomatics.

Site Parameter	Units	Site A	Site B	Site C	Site D	Site E	Site F
A_c	m^2	198	649	82	520	277	537
A_{max}	m^2	116	131	120	117	120	150
p-shape	-	0.95	0.61	1.00	1.67	1.45	1.30
h_0	m	0.49	0.71	0.65	0.47	0.38	0.52

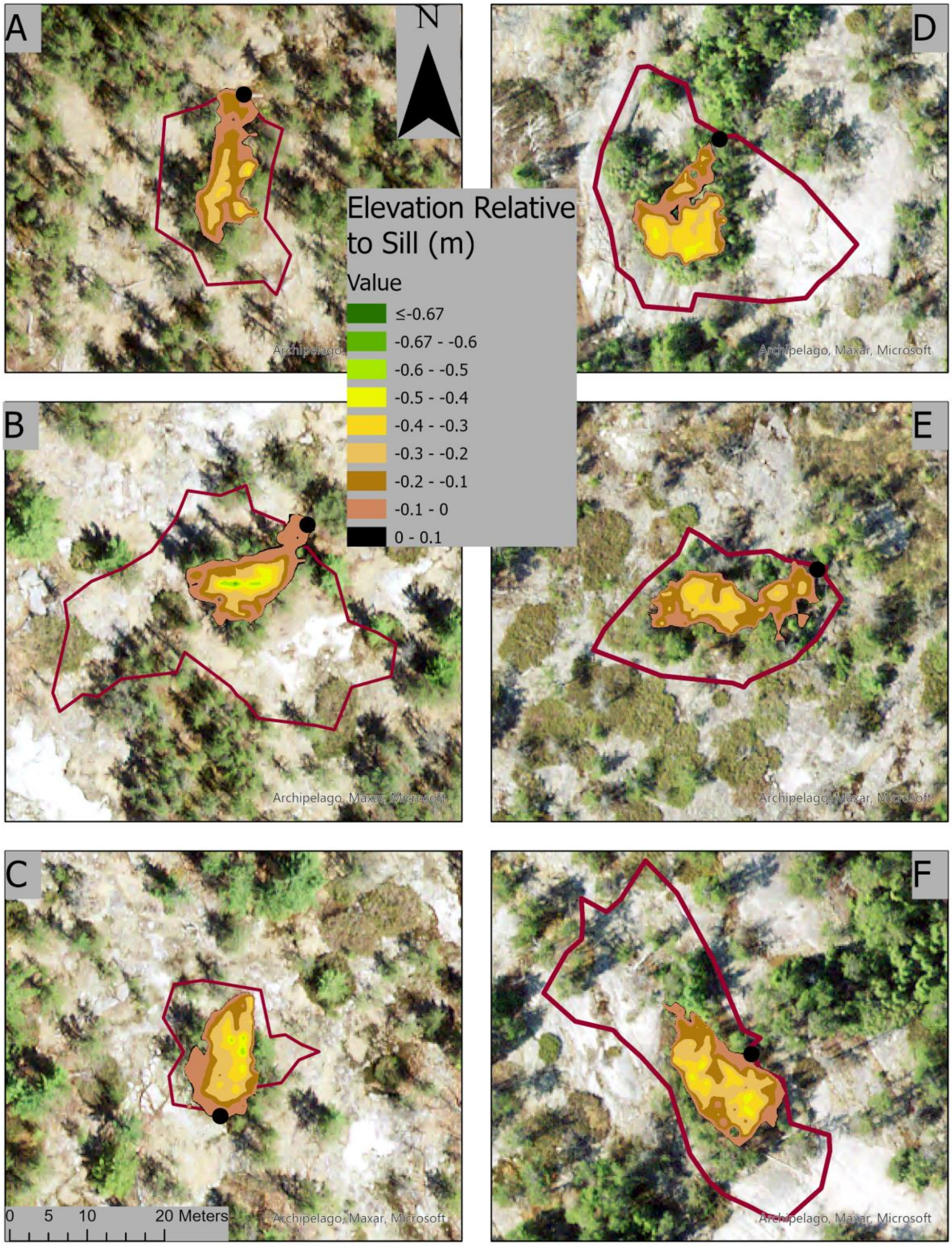

Figure 4. Bedrock morphometry within peat-filled depressions and delineated watersheds (outlined in maroon) for unburned (A-C) and burned (D-F) sites. Black dots indicate where the depression sills are located. Background imagery is from COOP and taken in 2016 (pre-fire).

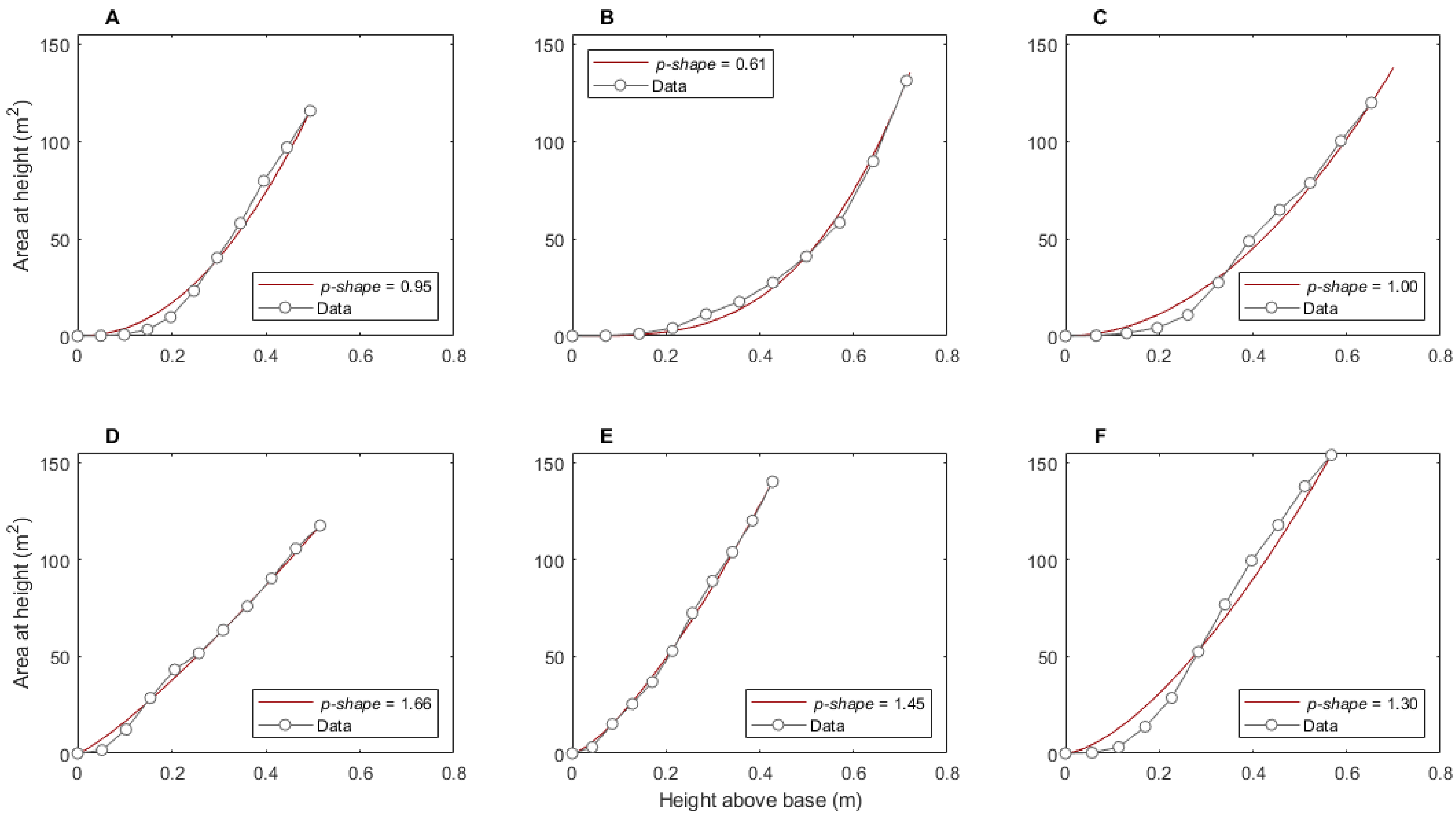

Figure 5. A-h method fits for *p-shape* parameter for unburned (A-C) and burned (D-F) sites using the equation provided in Hayashi & van der Kamp (2000).

Calibration/Validation

Table 6. Calibrated Parameters values and RMSE from the calibration and validation at each unburned site. Calibration RMSE is further broken into the RMSE for 2017 and 2018 separately.

Parameter/Metric	Units	Site A	Site B	Site C
RMSE* (m)	m	0.0388	0.0652	0.0770
(2017)		(0.0252)	(0.0368)	(0.0368)
(2018)		(0.0510)	(0.0878)	(0.1068)
Validation RMSE	m	0.0588	0.1516	0.1164
WSS_{max}	m	0.4546	0.2449	0.3559
r_{min}	-	0.0529	0.0810	0.0785
r_{max}	-	0.9156	0.3782	0.9951
k	-	1.5362	1.561	0.5898
W_{outlet}	m	0.0032	0.0031	0.0482
Sy_{max}	-	0.7665	0.8649	0.8714
Sy_{slope}	-	5.0011	4.5731	4.6406

Of the sites calibrated in RHO (A-C), site A had the best performance from its optimum parameter set with RMSEs of 0.039 and 0.059 m for the calibration and validation, respectively. Sites B and C had higher RMSEs of 0.065 and 0.077 m, respectively, for the calibration and 0.152 and 0.116 m, respectively, for the validation. All sites had considerably lower RMSEs for 2017 compared to 2018, which is likely due to the WT remaining nearer the surface in 2017 (a “wet” year) and thus absolute differences in observed and modelled WTs were limited when compared to 2018 (and 2019) data (Table 6; Figures 6-9).

When comparing observed and modelled data in scatter plots points cluster nearer to the 1:1 line when the WT is at or near the elevation of the sill as opposed to lower WT positions (Figures 7 & 9). This indicates that the model is best at predicting the WT when the site is near or above the threshold to spilling and thus the parameterized model can be used to accurately predict the patterns of hydrological connectivity between depressions and the downstream landscape as this is when sites would be spilling.

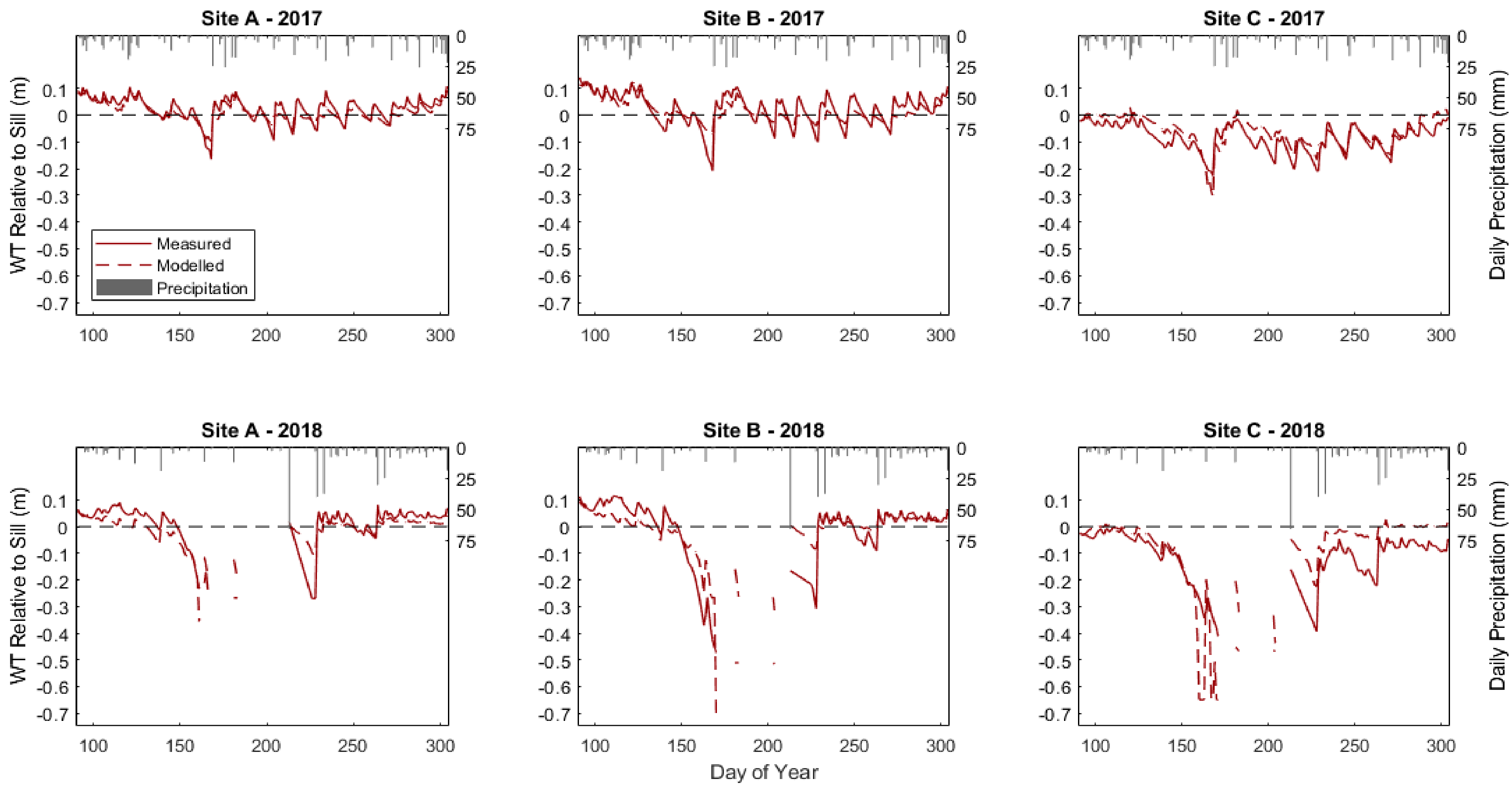

Figure 6. Observed (solid) and modelled (dashed) WT from calibration procedure for all unburned modelled depressions for 2017 (top) and 2018 (bottom). Gaps represent periods where the observed WT was considered lost and modelled WT was below the minimum observed WT.

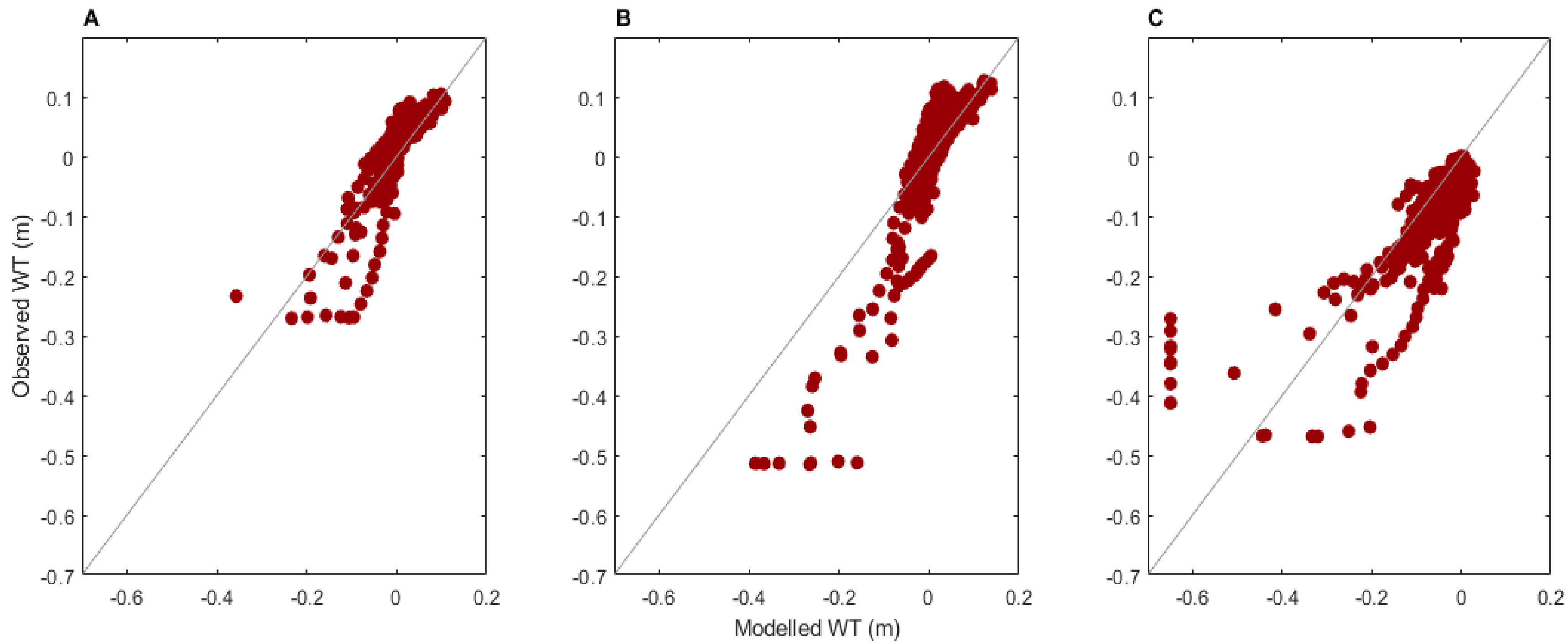

Figure 7. Scatter plots of observed (y-axis) vs modelled (x-axis) WT from the optimum parameter sets for 2017 and 2018, where grey lines are 1:1 lines, for each calibrated site.

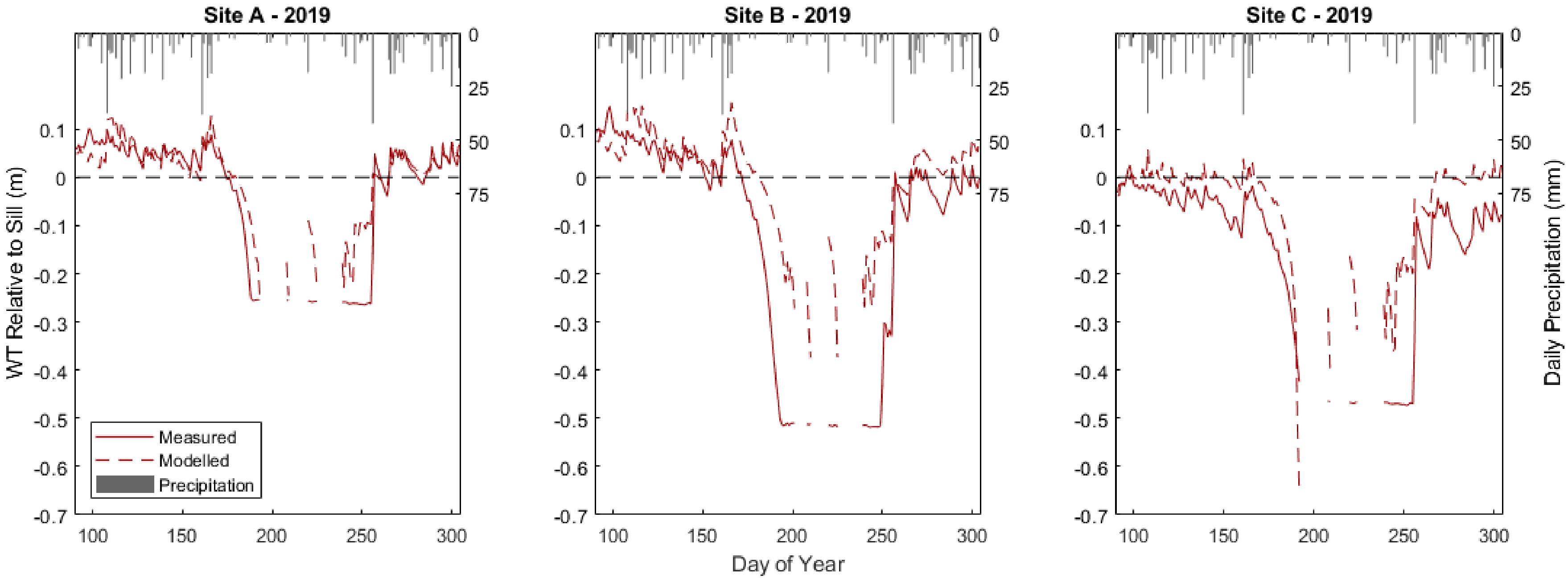

Figure 8. Observed (solid) and modelled (dashed) WT from validation of optimum parameter sets for all unburned modelled depressions for 2019. Gaps represent periods where the observed WT was considered lost and modelled WT was below the minimum observed WT.

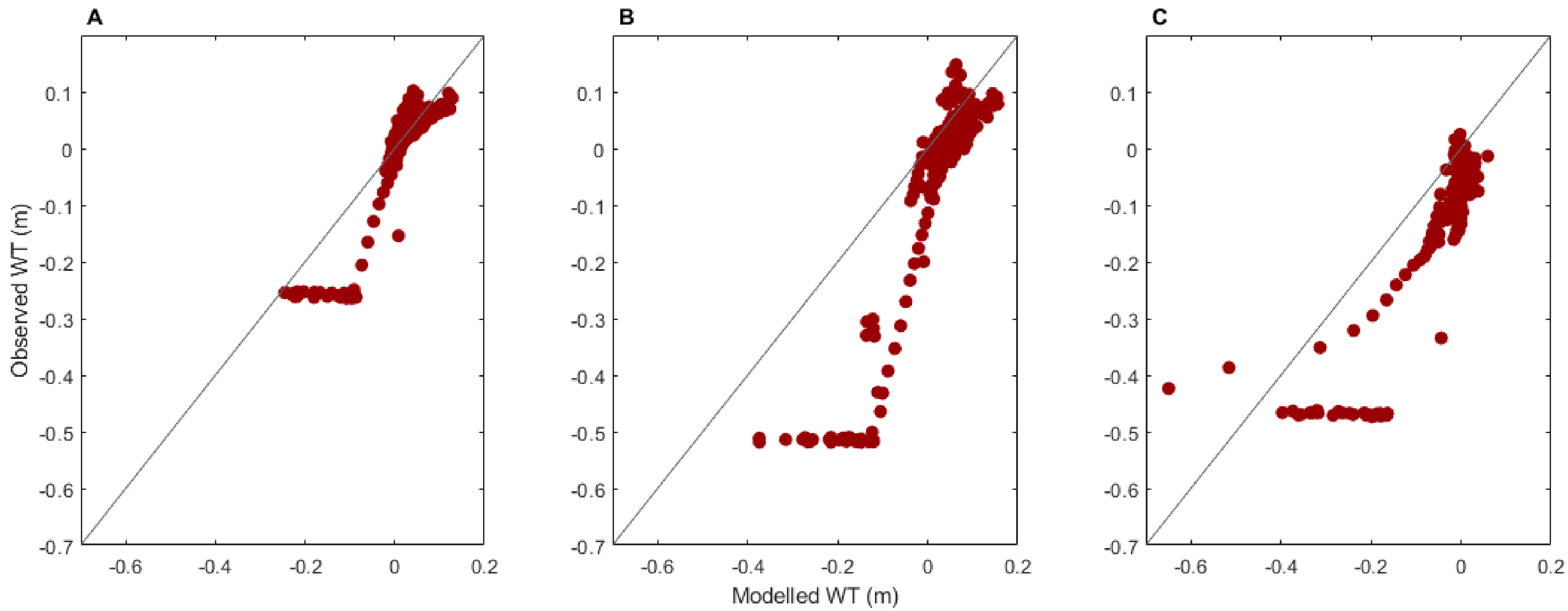

Figure 9. Observed (y-axis) vs modelled (x-axis) WT from validation runs for each site for 2019, where grey lines are 1:1 lines.

Parameter Uncertainty

For site A, RMSE is significantly ($p < 0.05$) correlated with r_{min}, r_{max}, k, and W_{outlet}. r_{min} and W_{outlet} have the strongest correlation coefficients at 0.47 and 0.39, respectively (Table 7; Figure 10). RMSE is only significantly correlated with r_{min} and W_{outlet} in site B, with correlation coefficients of 0.26 and 0.22, respectively (Table 7; Figure 11). Finally, site C exhibits different behaviour compared to sites A and B. Every parameter for site C is significantly correlated with RMSE except for W_{outlet}. The parameters and their correlation coefficients in descending magnitude are r_{min} (0.45), Sy_{slope} (0.45), Sy_{max} (-0.32), r_{max} (0.23), k (0.17), and WSS_{max} (-0.16) (Table 7; Figure 12). Site C is the only site with significant correlations for WSS_{max}, Sy_{max}, and Sy_{slope}.

The direction of the correlation for a given parameter was not consistent across sites, however when two or all three sites have significant correlations for the same parameter, they share the same direction. It is also important to note that the direction of the correlation does not necessarily correspond with, or indicate, what the optimum parameter value would be. For example, r_{max} and RMSE are significantly correlated in site A with a correlation coefficient of 0.24 (Table 7; Figure 10). This positive correlation indicates that as r_{max} becomes larger RMSE should also become larger or that smaller r_{max} values should result in the best model performance. However, the optimum r_{max} value for site A is 0.92 (Table 6) which is near the upper part of the parameter range, and in referring to the scatter plots the best performances (lowest RMSEs) come from r_{max} values as they get larger.

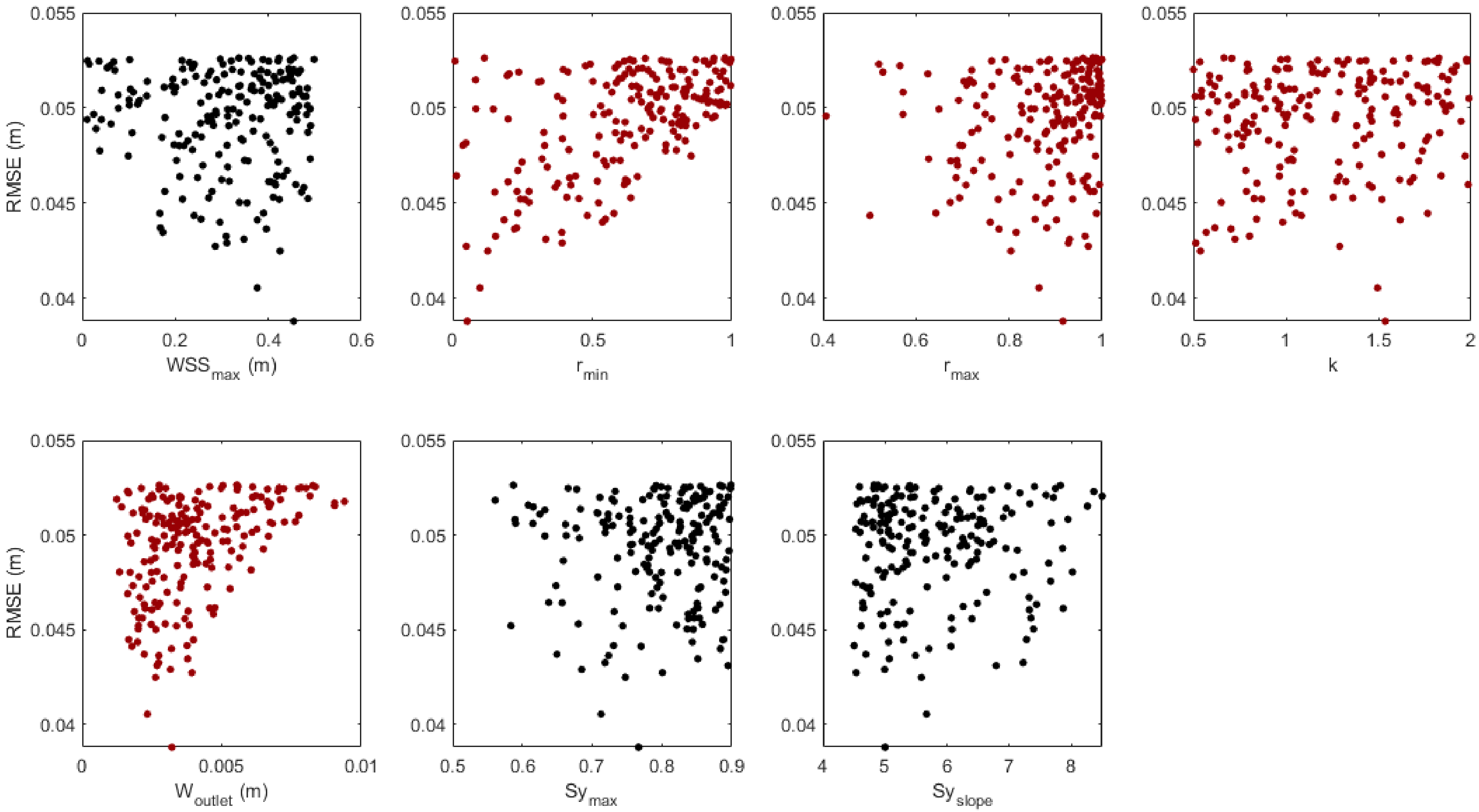

Figure 10. Model performance, according to RMSE, of the top 1% of parameter sets against each calibrated parameter for site A. Figures in maroon represent significant ($p < 0.05$) Spearman rank correlations.

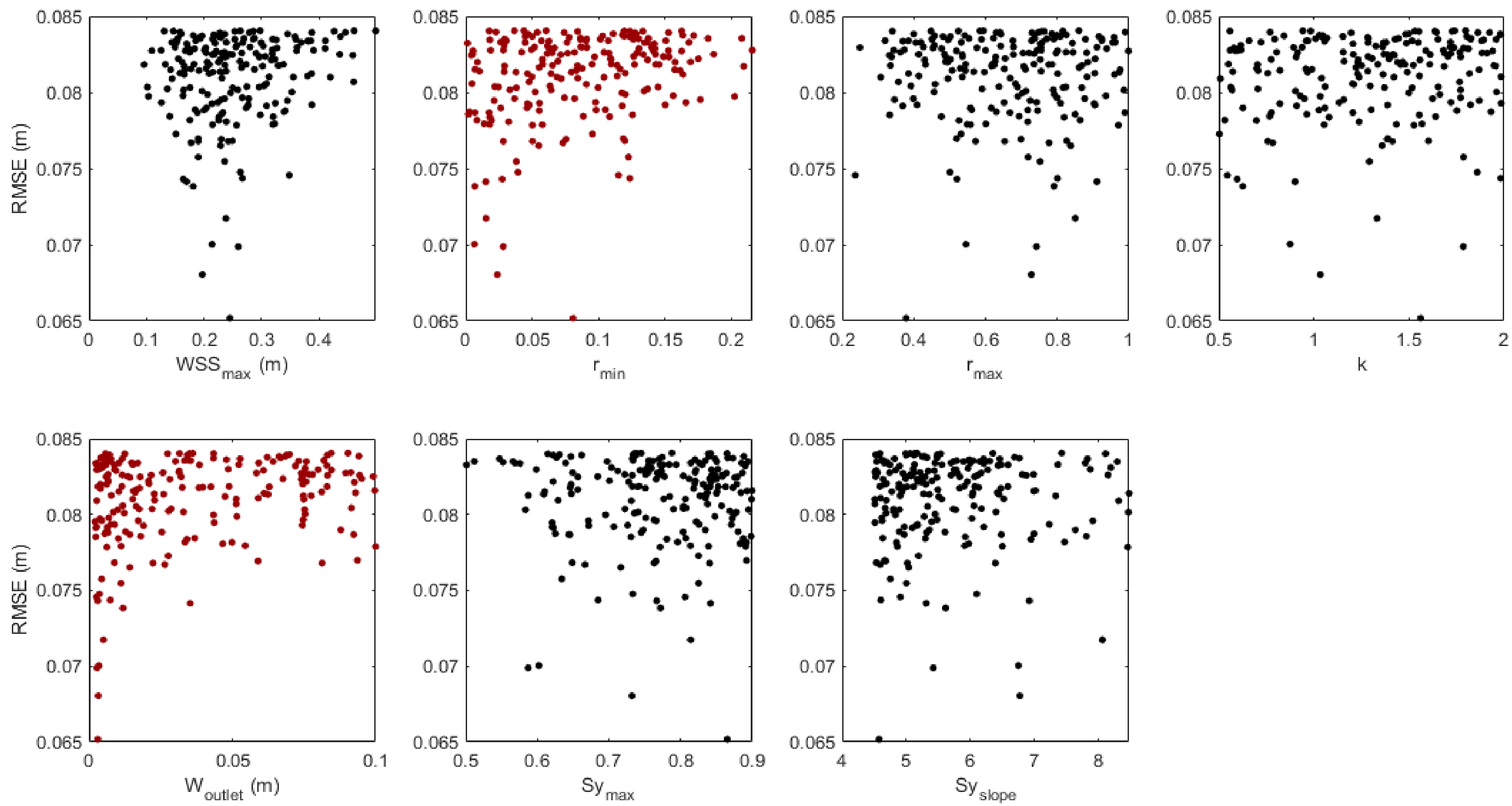

Figure 11. Model performance, according to RMSE, of the top 1% of parameter sets against each calibrated parameter for site B. Figures in maroon represent significant ($p < 0.05$) Spearman rank correlations.

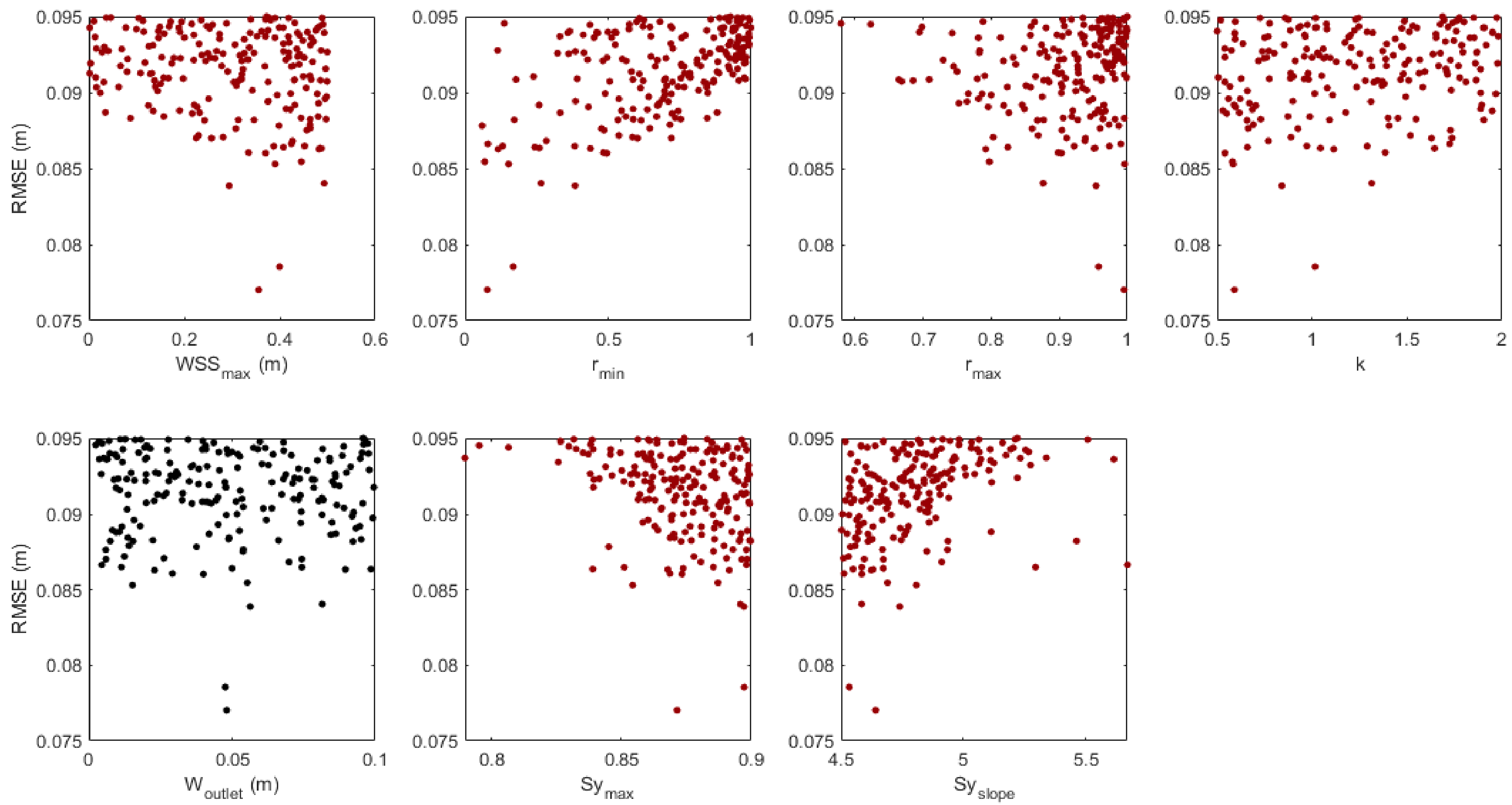

Figure 12. Model performance, according to RMSE, of the top 1% of parameter sets against each calibrated parameter for site C. Figures in maroon represent significant ($p < 0.05$) Spearman rank correlations.

Table 7. Spearman rank correlation coefficients and associate p-values for RMSE against each of the calibrated parameters for each site, using the top 1% of parameter sets. Significant ($p < 0.05$) correlations are denoted in maroon.

Parameter	Site A	p-value	Site B	p-value	Site D	p-value
WSS_{max}	-0.0033	0.9630	0.1225	0.0840	-0.1566	0.0269
r_{min}	0.4686	1.7E-12	0.2559	2.7E-04	0.4534	2.0E-11
r_{max}	0.2402	6.3E-04	-0.0228	0.7487	0.2341	8.8E-04
k	0.1401	0.0479	0.1183	0.0953	0.1663	0.0187
W_{outlet}	0.3939	1.1E-08	0.2235	0.0015	-0.0684	0.3355
Sy_{max}	0.0542	0.4458	-0.0549	0.4397	-0.3191	4.6E-06
Sy_{slope}	0.0431	0.5442	0.0348	0.6244	0.4480	4.0E-11

Basic Scenario Test

For the initial scenario tests examining both combined and separate impacts to run-in and DOB, a Kruskal-Wallis test found significant differences in connectedness index between the scenarios (df = 3, X^2 = 1434.83, p = 8.16x10^{-311}), where all burned scenarios have higher connectedness indices compared to the unburned scenario. The unburned scenario has a median connectedness index of 0.41 (± 0.006) compared to 0.77 (± 0.005), 0.45 (± 0.006), and 0.75 (± 0.005) in the fully burned, burned depression, and burned uplands scenarios respectively (Figure 13). The fully burned scenario and the burned uplands scenario are significantly different from the burned depression scenario, but not significantly different from each other.

One-at-a-Time Sensitivity Analysis

The stepwise sensitivity analysis shows that increasing all three impacted parameters results in an increase in the connectedness index from the model. The magnitude of the effect is most prominent when making changes to r_{min}, followed by r_{max}, and finally DOB. Within the bounds of the initial scenario test increases to r_{min}, while r_{max} and DOB are held constant, result in the largest increase in connectedness index, where the median connectedness index increases from 0.41 (± 0.006) at the unburned r_{min} of 0.05 to 0.64 (± 0.006) at an r_{min} of 0.25, while further increases in r_{min} result in increases in connectedness index up to 0.81 (± 0.004) at an r_{min} of 0.5 (Figure 14). Increasing r_{max} alone, from 0.7 to 1, results in connectedness index increasing from 0.41 (± 0.006) to 0.53 (± 0.006). Finally, connectedness index shows a threshold behaviour with increases to DOB, where connectedness index increases from 0.41 (± 0.006) at a DOB of 0 m to 0.46 (± 0.006) at a DOB of only 0.15 m after which further increases to DOB do not result in any further increases to connectedness (Figure 14).

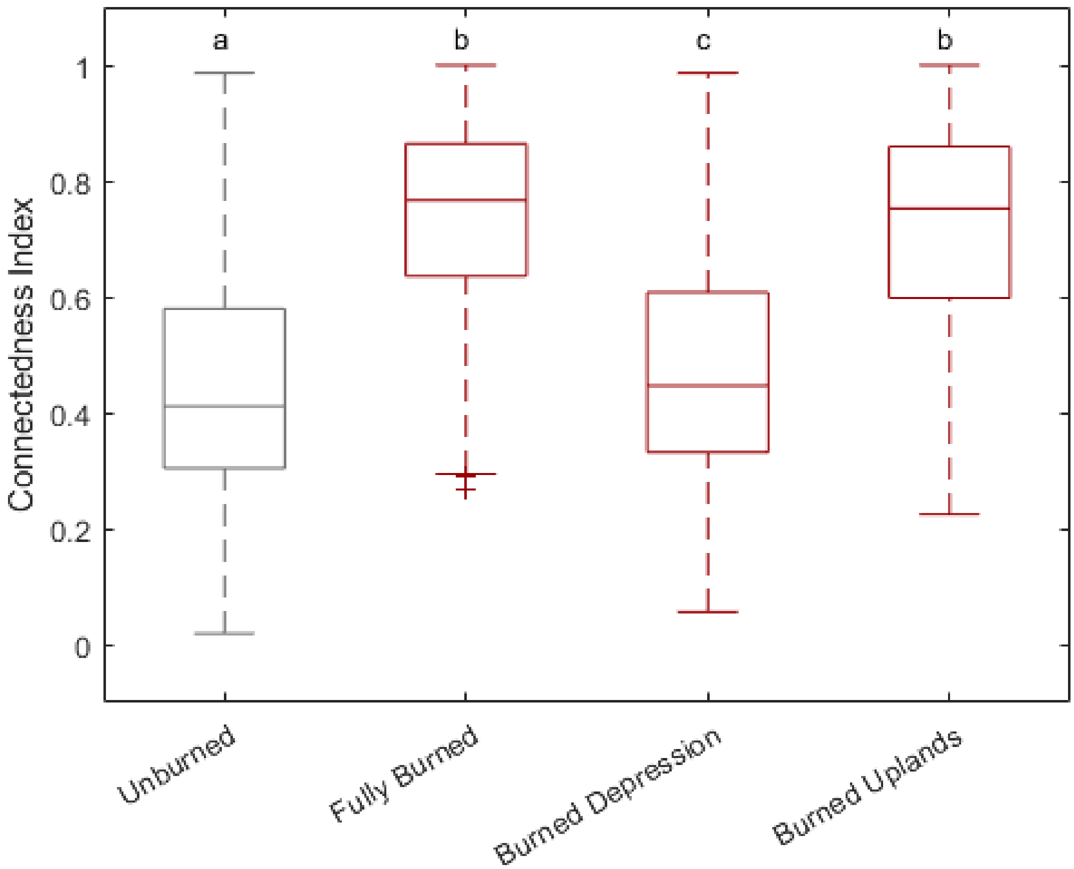

Figure 13. A box plot of connectedness index from 1000 model simulations of initial unburned (grey) and burned (maroon) scenario tests. Letters indicate statistically significant differences in connectedness index between scenarios according to the Kruskal-Wallis test.

.

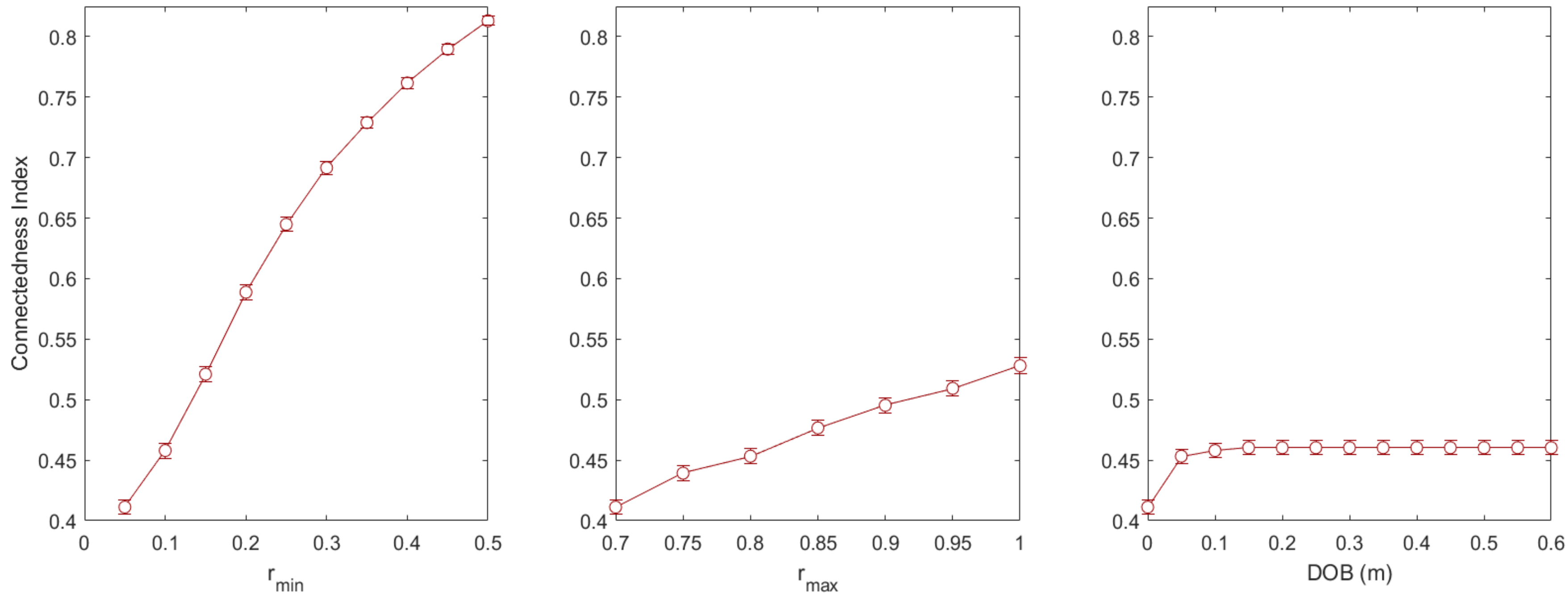

Figure 14. Median connectedness index, from 1000 simulations, for each testing value from the OAT sensitivity analysis for r_{min} (left), r_{max} (centre), and DOB (right). Error bars show the standard error.

<u>Factorial Scenario Test</u>

Median connectedness index and predicted total Q_{out} over the snow-free season increase from 0.41 and 245 mm, respectively in the unburned scenario, and up to 0.72 and 495 mm in the worst-case scenario in the factorial scenario testing (Figure 15&16). The median connectedness index and Q_{out} increase with any increase in the impacted parameters for a given depression under the same weather inputs. The median total Q_{in} increases with increases in r_{min} alone, r_{max} alone, and r_{min} and r_{max} together, but not with changes to DOB (Figure 17). Further, median total ET increases with increases to r_{min} alone, r_{max} alone, and r_{min} and r_{max} together, indicating more water is available within sites for ET (Figure 18). However, ET decreases with increases in DOB due to its dependence on the evaporative surface area (which decreases with increasing DOB).

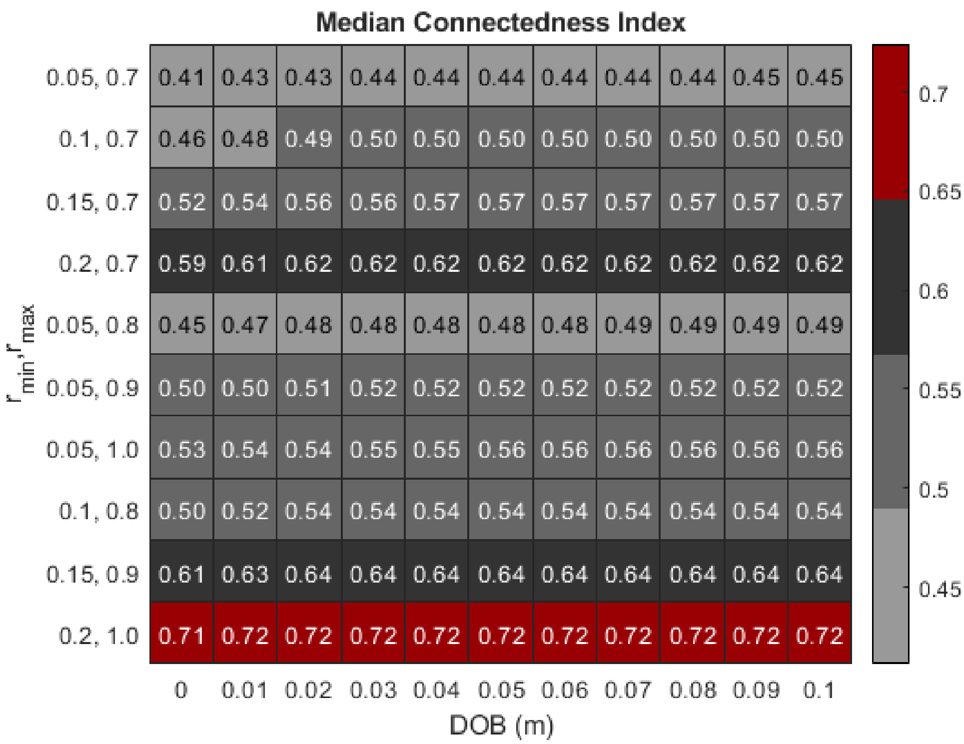

Figure 15. Median values of connectedness index from 1000 model simulations for each unique combination of input parameters tested in the factorial scenario test. The y-axis on each plot is the r_{min} and r_{max} value, and the x-axis is the DOB (m). Scale bar to the right of each plot indicates ranges used for colour values, and median values shown within squares.

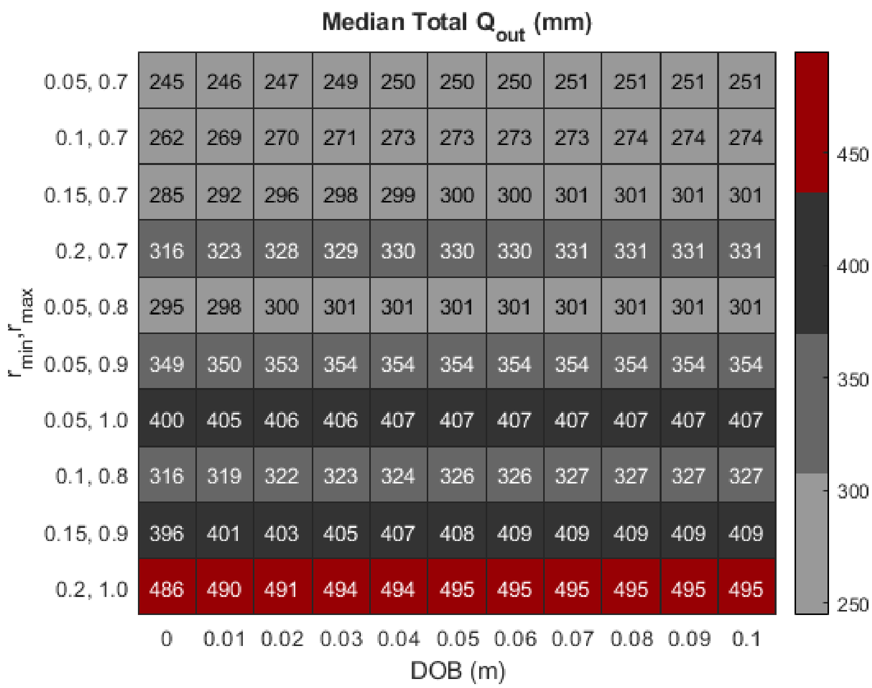

Figure 16. Median values of total Q_{out} (mm) from 1000 model simulations for each unique combination of input parameters tested in the factorial scenario test. The y-axis on each plot is the r_{min} and r_{max} value, and the x-axis is the DOB (m). Scale bar to the right of each plot indicates ranges used for colour values, and median values shown within squares.

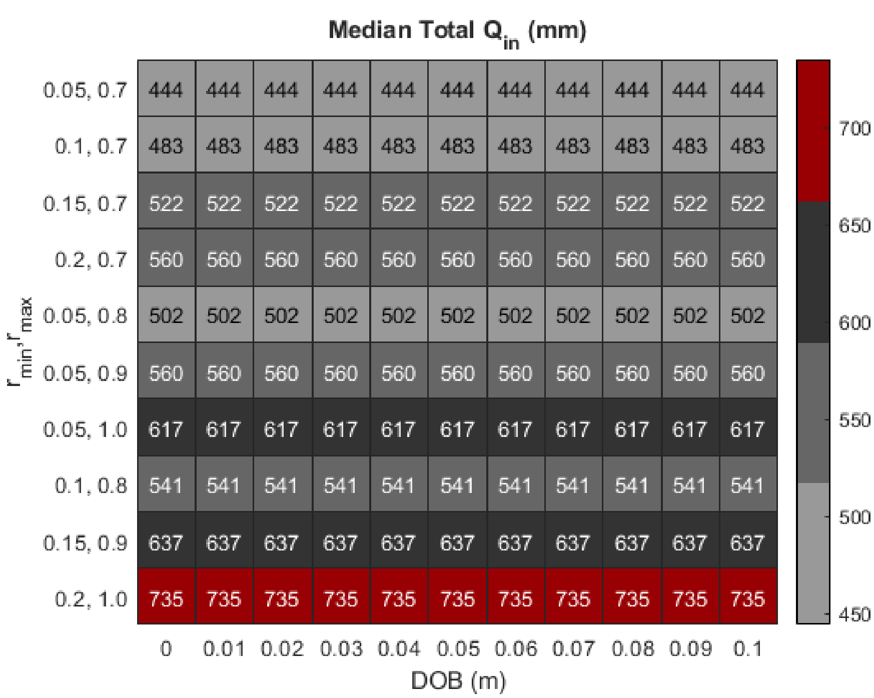

Figure 17. Median values of total Q_{in} (mm) from 1000 model simulations for each unique combination of input parameters tested in the factorial scenario test. The y-axis on each plot is the r_{min} and r_{max} value, and the x-axis is the DOB (m). Scale bar to the right of each plot indicates ranges used for colour values, and median values shown within squares.

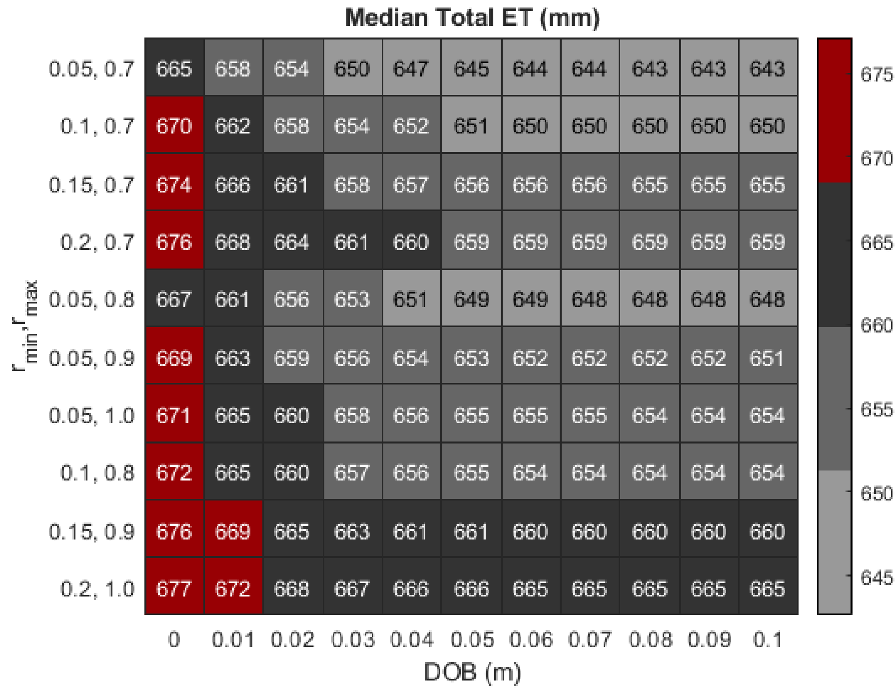

Figure 17. Median values of total ET (mm) from 1000 model simulations for each unique combination of input parameters tested in the factorial scenario test. The y-axis on each plot is the r_{min} and r_{max} value, and the x-axis is the DOB (m). Scale bar to the right of each plot indicates ranges used for colour values, and median values shown within squares.

CHAPTER 4: DISCUSSION

Bedrock depressions within Ontario's rock barrens landscape provide the conditions necessary to support several critical ecohydrological functions and act as a gatekeeper to landscape hydrological connectivity (Catling & Brownell, 1999). They store water on a landscape which generally has little to no soil to store water, enabling the development of wetlands and peat forming mosses (i.e., *Sphagnum*) and other wetland flora, which in turn provides a carbon storage function (Didemus, 2016; Furukawa, 2018). Moreover, the strong fill-and-spill hydrological dynamics of these depressions regulate the hydrological connectivity of the landscape and the aforementioned ecosystem services. We found that RHO, when parameterized for a given depression, can accurately predict water table (WT) behaviour (Figures 6-9) and in turn the hydrological connectivity of depressions and their upslope watersheds to the downstream landscape. The success of RHO supports the relatively simple assumptions regarding the lack of groundwater connection within these depressions (Catling & Brownell, 1999; Didemus, 2016).

Optimum calibrated parameter values from sites A-C tend to be similar across sites (Table 6), however, when parameter values do differ, one site tends to be different while the other two remain similar. For example, sites A and B have W_{outlet} values of 3.2 x 10^{-3} and 3.1 x 10^{-3} m, respectively while site C has an optimal W_{outlet} that is an order of magnitude larger at 4.82 x 10^{-2} m (Table 6). However, site C rarely has a WT at or above the sill (Figures 4-7), and therefore rarely spills and thus it is reasonable that a parameter which controls the rate of discharge in W_{outlet} has little impact on model performance. Essentially, any parameter value, provided it is large enough to allow for the free flow of water out of the depression, would be appropriate. This is also evident in the Spearman rank correlation coefficients, where calibration RMSE and W_{outlet} are significantly correlated for sites A and B but not for site C (Figures 10-12; Table 6). Further, r_{max} is much lower for site B than for sites A and C (Table 6), however site B has a much larger upslope watershed area than sites A and C (Table 5) which may be the cause of this difference. In addition, site C's much smaller upslope watershed area is likely to be the source of its much lower *k* value – one parameter related to Q_{in} (Tables 5&6). In summary, although there are considerable similarities in the calibrated parameter values between sites (Table 6) and RHO is able to accurately predict WT dynamics in each depression, in-depth field studies of hillslope hydrology and its underlying processes in the rock barrens will help clarify some of the parameter uncertainty and equifinality associated with the calibrated parameters (Figures 10-12). Further, the patchy ground cover and distribution of smaller depressions within the upslope watershed area, which also store water and exhibit fill-and-spill dynamics, may result in variability in the hydrological behaviour of individual watersheds (*e.g.*, Oswald et al., 2011). Hence a better understanding of how these watershed characteristics impact hydrology may be a further aid in modelling ungauged depressions.

The *p-shape* parameter and associated methods from Hayashi & van der Kamp (2000) are able to accurately represent the morphometry of the bedrock depressions in this study (Figure 5) with similar success and within the range of *p-shape* parameters found by Brooks & Hayashi (2002) – where *p-shape* ranged from 0.6 – 2.24 for forested vernal pools in Massachusetts. However, the intensive field surveys used to obtain this information along with the calibration procedure needed to obtain the necessary parameter values in this study do not currently allow for the use of RHO on ungauged basins. Consequently, a goal of future research should be determining the benefit of measuring difficult to obtain parameter values, such as depression morphometry, by assessing the variability of parameter values across a wider range of sites and determining the sensitivity of the model output of interest to input parameters. Further, determining the relationship between difficult to measure parameter values, which greatly improve model performance, to ones that are easy to obtain through less intensive field surveys or geomatics (*i.e.*, watershed ground cover to Q_{in} related parameters) will make the modelling of ungauged depressions more effective.

Between the selected ephemeral wetlands, field surveys show a wide range of maximum depths, bedrock morphometry, and watershed areas (Table 5), indicating potentially large variations in depression and watershed characteristics and in turn large variability in landscape hydrological function. However, more surveys of a wider selection of depressional wetlands would be necessary to draw conclusions regarding the distribution of landscape wide characteristics. Currently, mapping the location of depressional wetlands, their surface areas, and watershed characteristics are easily achieved through geomatics, however this is not capable of accurately assessing depression depth or morphometry.

There is potential for RHO to be adapted for use on ungauged depressions where it may serve as a significant component of a landscape wide hydrological model for the rock barrens landscape. Similar modelling efforts have been made for landscapes which contain ephemeral wetlands. For example, Evenson et al. (2018b) used the fill-and-spill concept to model surface and subsurface water flow using the SWAT-DSF model in the Greensboro watershed (a watershed in the Delmarva peninsula of Maryland dominated by depressional wetland HRUs) using high resolution spatial data of more than 1700 depressional HRUs within the watershed and successfully replicated streamflow and wetland inundation patterns. This modelling approach would be applicable within Ontario's rock barrens landscape, which is similarly dominated by depressional HRUs. This application would be useful both in the modelling of impacts such as wildfire and land use change, as well as predicting which parts of the landscape may be most vulnerable to disturbance under climate change. As disturbance vulnerability and impacts are often highly spatially variable (Wilkinson et al., 2019, 2020a, 2021), both are helpful applications as these disturbances are predicted to continue occurring and will likely intensify in the future (Flannigan et al., 2013; Niemi et al., 2007; Walton & Willeneuve, 1999).

Wildfire Scenario Testing

The impact of wildfire disturbance on landscape hydrology has been studied across North America (Moody et al., 2008; Pelster et al., 2008; Robinne et al., 2020; Silins et al., 2016), however studies specific to the rock barrens landscape are limited. The exploratory modelling scenarios in this study help reveal the potential changes to the water balance of ephemeral wetlands in Ontario's rock barrens landscape and how that in turn impacts the hydrological connectivity of the landscape.

In all scenarios tested in RHO, wildfire impacts led to increases in connectedness (Figure 13). The main impact to the connectedness of the modelled depression is from the increase in run-in from the upslope watershed area. Although it was hypothesized that the removal of peat through combustion (i.e., depth of burn; DOB) would lead to an increase in depression storage capacity and thus a reduction in connectedness, the model in fact shows that the connectedness index increases, albeit marginally, with increasing DOB up to 0.15 m of burning (Figure 14). This may be counterintuitive as the storage capacity of the depression does increase, however, as shown in the factorial scenario testing, the total evaporation from the depression decreases as DOB increases (Figure 18). This is because the evaporative surface becomes smaller as the peat surface recedes into the depression. This reduction in evaporation maintains higher storage levels, and counteracts the increases in storage capacity, causing the depression to become hydrologically connected more often.

The higher maintained WT and storage levels in burned depressions may have implications for the recovery of the ecosystems post-fire, and in turn, the reestablishment of ecosystem function and critical ecosystem services. These post-fire hydrological conditions indicate that burned depressions can maintain moist conditions and prevent the typical drying out seen in unburned ephemeral wetlands. This would in turn protect the remaining carbon stored in peat from further decomposition and subsequent burning and help maintain conditions conducive to vegetation recovery and carbon accumulation (Waddington et al., 2015). The increase in connectedness and discharge from upstream ephemeral wetlands would also help to maintain water levels in downstream wetlands and HRUs aiding in landscape-wide ecosystem recovery. In fact, McDonald (2021) showed that the burned rock barrens landscape acted as a carbon sink during the growing season only one to two years following fire.

Although this study aimed to examine the general impacts of wildfire on the water balance of ephemeral wetlands by testing changes to model parameters controlling the run-in and DOB, this does not incorporate the potentially significant changes to peat hydrophysical properties and peatland hydrology that are possible following wildfire. For example, peat soils are known to become hydrophobic following fire (Kettridge et al., 2014; Moore et al., 2017; Wilkinson et al., 2020b) which can create an evaporative barrier reducing evaporation from the peat surface (Kettridge et al., 2014), however this evaporative barrier can be broken in severe burning leading to an increase in surface evaporation (Wilkinson et al., 2020b). This modelling exercise also does not consider the changes in canopy cover that occur following wildfire, which can lead to decreases in transpiration, increases in surface evaporation, changes to boundary layer conditions, and increases in throughfall, all of which may have interacting changes to the water balance of ecosystems following disturbance (*e.g.,* Kettridge et al., 2013; Kettridge & Waddington, 2014). As mentioned, the modelled changes to the peat specific yield profile are conservative estimates as they do not account for any further changes to peat properties that are known to occur because of combustion (Sherwood et al., 2013), as such an examination of peat properties from burned wetlands in the rock barrens would help further inform changes to peat properties and in turn WT dynamics after wildfire disturbance. Further field studies may aid in future modelling exercises to further investigate the changes to the water balance and landscape hydrological connectivity.

Further research is also necessary to confirm the magnitude of change to run-in related parameters within the burned landscape, either through proper model calibration when there is the necessary data to do so, or through further field studies. The burned landscape also presents an opportunity to better understand the behaviour of runoff from rock barrens landscapes in general, by providing both a landscape with a lack of vegetation and soil to compare to unburned landscapes, as well as a landscape to observe the recovery of vegetation and soil patches and the impact of that recovery on depression and landscape wide water balances.

The modelling exercises in this study provide insight into the possible changes in the water balance of rock barrens ephemeral wetlands and the subsequent changes in hydrological connectivity. These exercises help in directing future studies on the changes to hydrology in the rock barrens landscape after disturbance and represent one possible application of a water balance model in predicting impacts from disturbance in the rock barrens.

CHAPTER 5: CONCLUSION

Bedrock depressions in Ontario's rock barrens landscape support the development of peat-filled, ephemeral wetlands due to the impermeable underlying bedrock and the absence of fracturing (Catling & Brownell, 1999; Didemus, 2016). These depressional wetlands exhibit strong fill-and-spill dynamics (Spence & Woo, 2003) which act as a significant control the hydrological connectivity between HRUs in rock barrens landscapes. Under low antecedent storage conditions depressions (and their upslope watershed areas) are disconnected from the rest of the landscape, however when storage is at or near depression storage capacity depressions quickly become connected to the rest of the landscape again, increasing the area contributing runoff from the landscape (Oswald et al., 2011; Spence & Woo, 2002, 2008). In this way depressional wetlands act as gatekeepers of landscape hydrological connectivity. The storage capacity and fill-and-spill dynamics are controlled by several wetland and watershed area characteristics, including the total volume of the depression, the hydrophysical properties of the peat, and the size and ability of the depression watershed to provide run-in.

Wildfire, although not extensively studied in Ontario's rock barrens landscape, is known to impact peat and landscape characteristics, through the removal of surficial moss and peat in peatlands (Wilkinson et al., 2020a) and increases to hillslope runoff (*e.g.* Silins et al., 2016) which is likely associated with reductions in storage capacity in upslope watershed areas that come along with large reduction in soil found after wildfire (Markle et al., 2020). The magnitude of these impacts, and the resulting changes to hydrological connectivity are yet unknown, however the use of models can aid in predicting the direction and magnitude of these changes.

Previous research has shown that simple water balance models and the fill-and-spill concept can be used to predict WT dynamics and hydrological connectivity in rock pools and depressional wetlands (Evenson et al., 2018b; Tuytens et al., 2014; Vanschoenwinkel et al., 2009). In addressing the first research objective we develop and parameterize a water balance model, RHO, through field surveys of depression morphometry, and the use of a calibration/validation procedure. We show that RHO can predict WT dynamics, and in turn the hydrological connectivity of ephemeral wetlands in the rock barrens landscape using precipitation and PET data from the snow-free season, when properly parameterized (Figures 6-9). We suggest future research to aid in further developing RHO for use in ungauged depressions and to adapt the modelling approaches used in RHO to model landscape-wide hydrological connectivity in rock barrens landscapes. RHO can therefore be further utilized to predict the potential impacts that wildfire disturbance may have on hydrological connectivity and subsequent ecosystem services in rock barrens landscapes.

For the second and third research objectives we used RHO to model changes to hydrological connectivity of ephemeral wetlands following wildfire by assessing (1) the magnitude and direction of change in hydrological connectivity associated with fire (objective 2) and (2) the relative contributions of impacts directly on the depression (through DOB) and to the upslope watershed area (through run-in related parameters) (objective 3). Four scenarios were set up, an unburned depression, a fully burned scenario where all impacted parameters were changed, a scenario in which only the DOB was changed, and finally a scenario in which only the run-in parameters were changed. This initial test showed that hydrological connectivity was significantly higher in all burn scenarios compared to the unburned scenario (Figure 13), and that changing only the run-in parameters resulted in a significantly higher increase in connectedness index compared to changing just the DOB (Figure 13). To further analyze these changes a one-at-a-time (OAT) sensitivity analysis was used, which showed that increases to r_{min} resulted in the greatest changes to hydrological connectivity, followed by increases to r_{max}. Increasing DOB resulted in minor increases in hydrological connectivity, until a DOB of 0.15 m after which there was no further change to connectivity (Figure 14). Finally, a factorial scenario test was used to break down the analysis, and to look at changes to other key water balance factors, namely total discharge (Q_{out}), total run-in (Q_{in}), and total ET. Q_{out} increased in accordance with changes to connectedness index, with an increase to any parameter resulting in an increase in Q_{out}. Further, Q_{in} increased with increases to run-in parameters (Figure 17). Changes to ET showed that increases in run-in parameters resulted in more water being made available to evaporate from the depression as median total ET increased. Interestingly median total ET decreased with increases to DOB due to the changes in the evaporative surface area associated with DOB (Figure 18), resulting in higher WT and connectedness index. This highlights an interesting feedback in post-fire water balance parameters and should form the basis of more detailed field-based studies.

To conclude, this thesis contributes to our understanding of the fill-and-spill dynamics of ephemeral wetlands in the rock barrens landscape through the development of a water balance model. This model was then used to investigate the impacts of wildfire disturbance to hydrological connectivity, which can help to inform how other ecosystems on the landscape and ecosystem services might be further impacted by changes to water supply and can be used to inform mitigation and restoration strategies following disturbance. This modelling approach has the potential to be expanded to landscape-wide modelling and include systems beyond ephemeral wetlands such as larger peatland systems in the rock barrens. Further, a water balance model such as RHO can be used to predict and better understand impacts from other disturbances, such as land use change and climate change. Future research should aim to determine the importance of difficult to measure parameters so RHO can be applied more generally across depression-dominated systems and should focus on further constraining free parameters that required calibration, specifically those associated with hillslope runoff processes and wetland discharge.

CHAPTER 6: REFERENCES

Alexander, M. E. (1980). Forest Fire History Research in Ontario: A Problem Analysis. In M. A. Stokes & J. H. Dieterich (Eds.), *Proceedings of the Fire History Workshop* (pp. 96–109). U.S. Department of Agriculture.

Ali, G., Oswald, C., Spence, C., & Wellen, C. (2018). The T-TEL Method for Assessing Water, Sediment, and Chemical Connectivity. *Water Resources Research*, *54*(2), 634–662. https://doi.org/10.1002/2017WR020707

Allan, C. J., & Roulet, N. T. (1994). Runoff generation in zero-order precambrian shield catchments: The stormflow response of a heterogeneous landscape. *Hydrological Processes*, *8*(4), 369–388. https://doi.org/10.1002/hyp.3360080409

Allin, D., Stone, M., Silins, U., Emelko, M. B., & Collins, A. L. (2012). The effects of wildfire on sediment-associated phosphorus forms in the Crowsnest River basin, Alberta, Canada. *Wildfire and Water Quality: Processes, Impacts and Challenges*, *354*, 11–14.

Beatty, S. M., & Smith, J. E. (2013). Dynamic soil water repellency and infiltration in post-wildfire soils. *Geoderma*, *192*, 160–172. https://doi.org/10.1016/J.GEODERMA.2012.08.012

Benavides-Solorio, J., & MacDonald, L. H. (2001). Post-fire runoff and erosion from simulated rainfall on small plots, Colorado Front Range. *Hydrological Processes*, *15*(15), 2931–2952. https://doi.org/10.1002/hyp.383

Benscoter, B. W., & Wieder, R. K. (2003). Variability in organic matter lost by combustion in a boreal bog during the 2001 Chisholm fire. *Canadian Journal of Forest Research*, *33*(12), 2509–2513. https://doi.org/10.1139/x03-162

Bladon, K. D., Emelko, M. B., Silins, U., & Stone, M. (2014). Wildfire and the Future of Water Supply. *Environmental Science & Technology*, *48*(16), 8936–8943.

https://doi.org/10.1021/es500130g

Bladon, K. D., Silins, U., Wagner, M. J., Stone, M., Emelko, M. B., Mendoza, C. A., Devito, K. J., & Boon, S. (2008). Wildfire impacts on nitrogen concentration and production from headwater streams in southern Alberta's Rocky Mountains. *Canadian Journal of Forest Research*, *38*(9), 2359–2371. https://doi.org/10.1139/X08-071

Bond-Lamberty, B., Peckham, S. D., Gower, S. T., & Ewers, B. E. (2009). Effects of fire on regional evapotranspiration in the central Canadian boreal forest. *Global Change Biology*, *15*(5), 1242–1254. https://doi.org/10.1111/j.1365-2486.2008.01776.x

Bracken, L. J., & Croke, J. (2007). The concept of hydrological connectivity and its contribution to understanding runoff-dominated geomorphic systems. *Hydrological Processes*, *21*(13), 1749–1763. https://doi.org/10.1002/hyp.6313

Branfireun, B. A., & Roulet, N. T. (1998). The baseflow and storm flow hydrology of a precambrian shield headwater peatland. *Hydrological Processes*, *12*(1), 57–72. https://doi.org/10.1002/(SICI)1099-1085(199801)12:1<57::AID-HYP560>3.0.CO;2-U

Brooks, R. T., & Hayashi, M. (2002). Depth-area-volume and hydroperiod relationships of ephemeral (vernal) forest pools in Southern New England. *Wetlands*, *22*(2), 247–255. https://doi.org/10.1672/0277-5212(2002)022[0247:DAVAHR]2.0.CO;2

Burles, K., & Boon, S. (2011). Snowmelt energy balance in a burned forest plot, Crowsnest Pass, Alberta, Canada. *Hydrological Processes*, *25*, 3012–3029. https://doi.org/10.1002/hyp.8067

Catling, P. M., & Brownell, V. R. (1999). *The flora and ecology of Southern Ontario granite barrens* (pp. 392–405). Cambridge University Press.

DeBano, L. . (2000). The role of fire and soil heating on water repellency in wildland environments: a review. *Journal of Hydrology*, *231–232*, 195–206.

https://doi.org/10.1016/S0022-1694(00)00194-3

Didemus, B. (2016). *Water storage dynamics in peat-filled depressions of canadian shield rock barrens: implications for primary peat formation*. McMaster University, Hamilton.

Dixon, S. J., Kettridge, N., Moore, P. A., Devito, K. J., Tilak, A. S., Petrone, R. M., Mendoza, C. A., & Waddington, J. M. (2017). Peat depth as a control on moss water availability under evaporative stress. *Hydrological Processes*, *31*(23), 4107–4121. https://doi.org/10.1002/hyp.11307

Doerr, S. H., Shakesby, R. A., & Walsh, R. P. D. (2000). Soil water repellency: its causes, characteristics and hydro-geomorphological significance. *Earth-Science Reviews*, *51*(1–4), 33–65. https://doi.org/10.1016/S0012-8252(00)00011-8

Ebel, B. A., Moody, J. A., & Martin, D. A. (2012). Hydrologic conditions controlling runoff generation immediately after wildfire. *Water Resources Research*, *48*(3). https://doi.org/10.1029/2011WR011470

Environment and Climate Change Canada. (2019). *Historical Data - Climate - Environment and Climate Change Canada*. https://climate.weather.gc.ca/historical_data/search_historic_data_e.html

Evenson, G. R., Golden, H. E., Lane, C. R., McLaughlin, D. L., & D'Amico, E. (2018). Depressional wetlands affect watershed hydrological, biogeochemical, and ecological functions. *Ecological Applications*, *28*(4), 953–966. https://doi.org/10.1002/eap.1701

Evenson, G. R., Jones, C. N., McLaughlin, D. L., Golden, H. E., Lane, C. R., DeVries, B., Alexander, L. C., Lang, M. W., McCarty, G. W., & Sharifi, A. (2018). A watershed-scale model for depressional wetland-rich landscapes. *Journal of Hydrology X*, *1*, 100002. https://doi.org/10.1016/j.hydroa.2018.10.002

Ferguson, R. I., Sharma, B. P., Hardy, R. J., Hodge, R. A., & Warburton, J. (2017). Flow resistance and hydraulic geometry in contrasting reaches of a bedrock channel. *Water Resources Research*, *53*(3), 2278–2293. https://doi.org/10.1002/2016WR020233

Flannigan, M. D., Cantin, A. S., De Groot, W. J., Wotton, M., Newbery, A., & Gowman, L. M. (2013). Global wildland fire season severity in the 21st century. *Forest Ecology and Management*, *294*, 54–61. https://doi.org/10.1016/j.foreco.2012.10.022

Flannigan, M. D., Logan, K. A., Amiro, B. D., Skinner, W. R., & Stocks, B. J. (2005). Future Area Burned in Canada. *Climatic Change*, *72*(1–2), 1–16. https://doi.org/10.1007/s10584-005-5935-y

Flannigan, M. D., & Wagner, C. E. Van. (1991). Climate change and wildfire in Canada. *Canadian Journal of Forest Research*, *21*(1), 66–72. https://doi.org/10.1139/x91-010

Flannigan, M. D., Wotton, B. M., Marshall, G. A., de Groot, W. J., Johnston, J., Jurko, N., & Cantin, A. S. (2016). Fuel moisture sensitivity to temperature and precipitation: climate change implications. *Climatic Change*, *134*(1–2), 59–71. https://doi.org/10.1007/s10584-015-1521-0

Flügel, W. A. (1995). Delineating hydrological response units by geographical information system analyses for regional hydrological modelling using PRMS/MMS in the drainage basin of the River Bröl, Germany. *Hydrological Processes*, *9*(3–4), 423–436. https://doi.org/10.1002/hyp.3360090313

Frandsen, W. H. (1987). The influence of moisture and mineral soil on the combustion limits of smoldering forest duff. *Canadian Journal of Forest Research*, *17*(12), 1540–1544. https://doi.org/10.1139/x87-236

Frisbee, M. D., Allan, C. J., Thomasson, M. J., & Mackereth, R. (2007). Hillslope hydrology and wetland response of two small zero-order boreal catchments on the Precambrian Shield. *Hydrological Processes*, *21*(22), 2979–2997. https://doi.org/10.1002/hyp.6521

Furukawa, A. (2018). *Pore-Water Feedbacks and Resilience To Decay in Peat-Filled Depressions of the Canadian Shield*. McMaster Unviersity, Hamilton.

Greene, D. F., & Johnson, E. A. (1999). Modelling recruitment of Populus tremuloides, Pinus banksiana, and Picea mariana following fire in the mixedwood boreal forest. *Canadian Journal of Forest Research*, *29*(4), 462–473. https://doi.org/10.1139/x98-211

Hallema, D. W., Sun, G., Caldwell, P. V., Norman, S. P., Cohen, E. C., Liu, Y., Bladon, K. D., & McNulty, S. G. (2018). Burned forests impact water supplies. *Nature Communications*, *9*(1). https://doi.org/10.1038/s41467-018-03735-6

Hanes, C. C., Wang, X., Jain, P., Parisien, M. A., Little, J. M., & Flannigan, M. D. (2019). Fire-regime changes in Canada over the last half century. *Canadian Journal of Forest Research*, *49*(3). https://doi.org/10.1139/cjfr-2018-0293

Hayashi, M., & van der Kamp, G. (2000). Simple equations to represent the volume-area-depth relations of shallow wetlands in small topographic depressions. *Journal of Hydrology*, *237*(1–2), 74–85. https://doi.org/10.1016/S0022-1694(00)00300-0

Hokanson, K. J., Lukenbach, M. C., Devito, K. J., Kettridge, N., Petrone, R. M., & Waddington, J. M. (2016). Groundwater connectivity controls peat burn severity in the boreal plains. *Ecohydrology*, *9*(4), 574–584. https://doi.org/10.1002/eco.1657

Hudson, D. T., Markle, C. E., Harris, L. I., Moore, P. A., & Waddington, J. M. (2020). Ecohydrological controls on lichen and moss CO2 exchange in rock barrens turtle nesting habitat. *Ecohydrology*, *May*, 1–11. https://doi.org/10.1002/eco.2255

Hulsmans, A., Vanschoenwinkel, B., Pyke, C., Riddoch, B. J., & Brendonck, L. (2008).

Quantifying the hydroregime of a temporary pool habitat: A modelling approach for ephemeral rock pools in SE Botswana. *Ecosystems*, *11*(1), 89–100. https://doi.org/10.1007/s10021-007-9110-3

IPCC. (2014). *Climate Change 2014: Impacts, Adaptation, and Vulnerability. In Contribution of Working Group II to the Fifth Assessment Report of the Intergovernmental Panel on Climate Change* (C. B. Field, V. R. Barros, D. J. Dokken, K. J. Mach, M. D. Mastrandrea, T. E. Bilir, M. Chatterjee, K. L. Ebi, Y. O. Estrada, R. C. Genova, B. Girma, E. S. Kissel, A. N. Levy, S. MacCracken, P. R. Mastrandrea, & L. L. White (Eds.)). Cambridge University Press.

Joon Kim, & Verma, S. B. (1996). Surface exchange of water vapour between an open sphagnum fen and the atmosphere. *Boundary-Layer Meteorology*, *79*(3), 243–264. https://doi.org/10.1007/bf00119440

Kettridge, N., Humphrey, R. E., Smith, J. E., Lukenbach, M. C., Devito, K. J., Petrone, R. M., & Waddington, J. M. (2014). Burned and unburned peat water repellency: Implications for peatland evaporation following wildfire. *Journal of Hydrology*, *513*, 335–341. https://doi.org/10.1016/J.JHYDROL.2014.03.019

Kettridge, N., Lukenbach, M. C., Hokanson, K. J., Devito, K. J., Petrone, R. M., Mendoza, C. A., & Waddington, J. M. (2019). Severe wildfire exposes remnant peat carbon stocks to increased post-fire drying. *Scientific Reports*, *9*(1), 3727. https://doi.org/10.1038/s41598-019-40033-7

Kettridge, N., Lukenbach, M. C., Hokanson, K. J., Hopkinson, C., Devito, K. J., Petrone, R. M., Mendoza, C. A., & Waddington, J. M. (2017). Low evapotranspiration enhances the resilience of peatland carbon stocks to fire. *Geophysical Research Letters*, *44*(18), 9341–9349. https://doi.org/10.1002/2017GL074186

Kettridge, N., Thompson, D. K., Bombonato, L., Turetsky, M. R., Benscoter, B. W., &

Waddington, J. M. (2013). The ecohydrology of forested peatlands: Simulating the effects of tree shading on moss evaporation and species composition. *Journal of Geophysical Research: Biogeosciences*, *118*(2), 422–435. https://doi.org/10.1002/jgrg.20043

Kettridge, N., & Waddington, J. M. (2014). Towards quantifying the negative feedback regulation of peatland evaporation to drought. *Hydrological Processes*, *28*(11). https://doi.org/10.1002/hyp.9898

Kirkby, M., Bracken, L., & Reaney, S. (2002). The influence of land use, soils and topography on the delivery of hillslope runoff to channels in SE Spain. *Earth Surface Processes and Landforms*, *27*(13), 1459–1473. https://doi.org/10.1002/esp.441

Larsen, I. J., MacDonald, L. H., Brown, E., Rough, D., Welsh, M. J., Pietraszek, J. H., Libohova, Z., de Dios Benavides-Solorio, J., & Schaffrath, K. (2009). Causes of Post-Fire Runoff and Erosion: Water Repellency, Cover, or Soil Sealing? *Soil Science Society of America Journal*, *73*(4), 1393–1407. https://doi.org/10.2136/sssaj2007.0432

Leibowitz, S. G., Mushet, D. M., & Newton, W. E. (2016). Intermittent Surface Water Connectivity: Fill and Spill Vs. Fill and Merge Dynamics. *Wetlands*, *36*. https://doi.org/10.1007/s13157-016-0830-z

Lukenbach, M. C., Devito, K. J., Kettridge, N., Petrone, R. M., & Waddington, J. M. (2016). Burn severity alters peatland moss water availability: implications for post-fire recovery. *Ecohydrology*, *9*(2), 341–353. https://doi.org/10.1002/eco.1639

Lukenbach, M. C., Hokanson, K. J., Moore, P. A., Devito, K. J., Kettridge, N., Thompson, D. K., Wotton, B. M., Petrone, R. M., & Waddington, J. M. (2015). Hydrological controls on deep burning in a northern forested peatland. *Hydrological Processes*, *29*(18). https://doi.org/10.1002/hyp.10440

Markle, C. E., Wilkinson, S. L., & Waddington, J. M. (2020). Initial effects of wildfire on freshwater turtle nesting habitat. *The Journal of Wildlife Management*, jwmg.21921. https://doi.org/10.1002/jwmg.21921

MATLAB (Version 9.8.0 (R2020a)). (2020). The MathWorks.

McDonald, R. (2021). *Boreal shield peatland CO2 exchange: A multi-year analysis and post-wildifre recovery assessment*. McMaster University, Hamilton.

Moody, J. A., Martin, D. A., Haire, S. L., & Kinner, D. A. (2008). Linking runoff response to burn severity after a wildfire. *Hydrological Processes*, *22*, 2063–2074. https://doi.org/10.1002/hyp.6806

Moody, J. A., Shakesby, R. A., Robichaud, P. R., Cannon, S. H., & Martin, D. A. (2013). Current research issues related to post-wildfire runoff and erosion processes. In *Earth-Science Reviews* (Vol. 122, pp. 10–37). https://doi.org/10.1016/j.earscirev.2013.03.004

Moore, P. A., Didemus, B. D., Furukawa, A. K., & Waddington, J. M. (2021). Peat depth as a control on Sphagnum moisture stress during seasonal drought. *Hydrological Processes*, *December 2020*, 1–12. https://doi.org/10.1002/hyp.14117

Moore, P. A., Lukenbach, M. C., Kettridge, N., Petrone, R. M., Devito, K. J., & Waddington, J. M. (2017). Peatland water repellency: Importance of soil water content, moss species, and burn severity. *Journal of Hydrology*, *554*, 656–665. https://doi.org/10.1016/J.JHYDROL.2017.09.036

Neary, D. G., Ryan, K. C., & DeBano, L. F. (2000). Wildland fire in ecosystems: Effects of fire on soils and water. In *Gen. Tech. Rep. RMRS-GTR-42-vol. 2. Ogden, UT: U.S. Department of Agriculture, Forest Service, Rocky Mountain Research Station*. https://doi.org/10.1111/j.1467-7717.2009.01106.x

Niemi, G. J., Kelly, J. R., & Danz, N. P. (2007). Environmental indicators for the coastal region of the North American Great Lakes: Introduction and prospectus. In *Journal of Great Lakes Research* (Vol. 33, Issue SPEC. ISS. 3, pp. 1–12). International Association of Great Lakes Research. https://doi.org/10.3394/0380-1330(2007)33[1:eiftcr]2.0.co;2

Oswald, C. J., Richardson, M. C., & Branfireun, B. A. (2011). Water storage dynamics and runoff response of a boreal Shield headwater catchment. *Hydrological Processes*, *25*(19), 3042–3060. https://doi.org/10.1002/hyp.8036

Pelster, D. E., Burke, J. M., & Prepas, E. E. (2008). Runoff and inorganic nitrogen export from Boreal Plain watersheds six years after wildfire and one year after harvest 1. *Journal of Environmental Engineering and Science*, *7*(Suppl. 1), S51–S61. https://doi.org/10.1139/S07-030

Phillips, R. W., Spence, C., & Pomeroy, J. W. (2011). Connectivity and runoff dynamics in heterogeneous basins. *Hydrological Processes*, *25*, 3061–3075. https://doi.org/10.1002/hyp.8123

Price, J. S. (1996). Hydrology and microclimate of a partly restored cutover bog, Quebec. *Hydrological Processes*, *10*(10), 1263–1272. https://doi.org/10.1002/(SICI)1099-1085(199610)10:10<1263::AID-HYP458>3.0.CO;2-1

Pringle, C. M. (2001). Hydrologic connectivity and the management of biological reserves: a global perspective. *Ecological Applications*, *11*(4), 981–998. https://doi.org/10.1890/1051-0761(2001)011[0981:HCATMO]2.0.CO;2

Pringle, C. M. (2003). What is hydrologic connectivity and why is it ecologically important? *Hydrological Processes*, *17*(13), 2685–2689. https://doi.org/10.1002/hyp.5145

Pyke, C. R. (2004). Simulating vernal pool hydrologic regimes for two locations in California, USA. *Ecological Modelling*, *173*(2–3), 109–127. https://doi.org/10.1016/j.ecolmodel.2003.08.014

Robinne, F.-N., Hallema, D. W., Bladon, K. D., & Buttle, J. M. (2020). Wildfire impacts on hydrologic ecosystem services in North American high-latitude forests: A scoping review. *Journal of Hydrology*, *581*. https://doi.org/10.1016/j.jhydrol.2019.124360

Shakesby, R. A., Doerr, S. H., & Walsh, R. P. D. (2000). The erosional impact of soil hydrophobicity: Current problems and future research directions. *Journal of Hydrology*, *231–232*, 178–191. https://doi.org/10.1016/S0022-1694(00)00193-1

Sherwood, J. H., Kettridge, N., Thompson, D. K., Morris, P. J., Silins, U., & Waddington, J. M. (2013). Effect of drainage and wildfire on peat hydrophysical properties. *Hydrological Processes*. https://doi.org/10.1002/hyp.9820

Shetler, G., Turetsky, M. R., Kane, E., & Kasischke, E. (2008). Sphagnum mosses limit total carbon consumption during fire in Alaskan black spruce forests. *Canadian Journal of Forest Research*, *38*(8), 2328–2336. https://doi.org/10.1139/X08-057

Shure, D. J., & Ragsdale, H. L. (1977). Patterns of Primary Succession on Granite Outcrop Surfaces. *Ecology*, *58*(5), 993–1006. https://doi.org/10.2307/1936920

Silins, U., Anderson, A., Bladon, K. D., Emelko, M. B., Stone, M., Spencer, S. A., Williams, C. H. S., Wagner, M. J., Martens, A. M., & Hawthorn, K. (2016). Southern Rockies Watershed Project. *The Forestry Chronicle*, *92*(01), 39–42. https://doi.org/10.5558/tfc2016-012

Silins, U., Bladon, K. D., Kelly, E. N., Esch, E., Spence, J. R., Stone, M., Emelko, M. B., Boon, S., Wagner, M. J., Williams, C. H. S., & Tichkowsky, I. (2014). Five-year legacy of wildfire and salvage logging impacts on nutrient runoff and aquatic plant, invertebrate, and fish productivity. *Ecohydrology*, *7*(6), 1508–1523. https://doi.org/10.1002/eco.1474

Silins, U., Stone, M., Emelko, M. B., & Bladon, K. K. (2009). Sediment production following severe wildfire and post-fire salvage logging in the Rocky Mountain headwaters of the Oldman River Basin, Alberta. *CATENA*, *79*(3), 189–197. https://doi.org/10.1016/J.CATENA.2009.04.001

Spence, C. (2000). The Effect of Storage on Runoff from a Headwater Subarctic Shield Basin. *Arctic*, *53*(3), 237–247. https://www.jstor.org/stable/40511908

Spence, C. (2007). On the relation between dynamic storage and runoff: A discussion on thresholds, efficiency, and function. *Water Resources Research*, *43*(12). https://doi.org/10.1029/2006WR005645

Spence, C., & Phillips, R. W. (2015). Refining understanding of hydrological connectivity in a boreal catchment. *Hydrological Processes*, *29*(16), 3491–3503. https://doi.org/10.1002/hyp.10270

Spence, C., & Woo, M. (2002). Hydrology of subarctic Canadian shield: bedrock upland. *Journal of Hydrology*, *262*(1–4), 111–127. https://doi.org/10.1016/S0022-1694(02)00010-0

Spence, C., & Woo, M. (2003). Hydrology of subarctic Canadian shield: soil-filled valleys. *Journal of Hydrology*, *279*(1–4), 151–166. https://doi.org/10.1016/S0022-1694(03)00175-6

Spence, C., & Woo, M. (2006). Hydrology of subarctic Canadian Shield: heterogeneous headwater basins. *Journal of Hydrology*, *317*(1–2), 138–154. https://doi.org/10.1016/J.JHYDROL.2005.05.014

Spence, C., & Woo, M. (2008). Hydrology of the Northwestern Subarctic Canadian Shield. In *Cold Region Atmospheric and Hydrologic Studies. The Mackenzie GEWEX Experience* (pp. 235–256). Springer Berlin Heidelberg. https://doi.org/10.1007/978-3-540-75136-6_13

Taylor, P. D., Fahrig, L., Henein, K., & Merriam, G. (1993). Connectivity Is a Vital Element of

Landscape Structure. *Oikos*, *68*(3), 571. https://doi.org/10.2307/3544927

Thompson, D. K., & Waddington, J. M. (2013). Peat properties and water retention in boreal forested peatlands subject to wildfire. *Water Resources Research*, *49*(6), 3651–3658. https://doi.org/10.1002/wrcr.20278

Tromp-van Meerveld, H. J., & McDonnell, J. J. (2006). Threshold relations in subsurface stormflow: 2. The fill and spill hypothesis. *Water Resources Research*, *42*(2). https://doi.org/10.1029/2004WR003800

Tuytens, K., Vanschoenwinkel, B., Waterkeyn, A., & Brendonck, L. (2014). Predictions of climate change infer increased environmental harshness and altered connectivity in a cluster of temporary pools. *Freshwater Biology*, *59*(5), 955–968. https://doi.org/10.1111/fwb.12319

Van Sleeuwen, M. (2006). *Natural fire regimes of Ontario* (p. 143). Queen's Printer for Ontario. http://www.ontarioparks.com/english/fire_research.html

Vanschoenwinkel, B., Hulsmans, A., De Roeck, E., De Vries, C., Seaman, M., & Brendonck, L. (2009). Community structure in temporary freshwater pools: Disentangling the effects of habitat size and hydroregime. *Freshwater Biology*, *54*(7), 1487–1500. https://doi.org/10.1111/j.1365-2427.2009.02198.x

Waddington, J. M., Morris, P. J., Kettridge, N., Granath, G., Thompson, D. K., & Moore, P. A. (2015). Hydrological feedbacks in northern peatlands. *Ecohydrology*, *8*, 113–127. https://doi.org/10.1002/eco.1493

Walton, M., & Willeneuve, M. (1999). Ecosystem planning in Georgian Bay Islands National Park: a multi-jurisdictional approach. In *Second International Symposium and Workshop on the Conservation of the Eastern Massasauga Rattlesnake, Sistrurus catenatus catenatus: Population and Habitat Management Issues in Urban, Bog, Prairie and Forested Ecosystems* (pp. 81–84). Toronto Zoo.

Wilkinson, S. L., Furukawa, A. K., Wotton, B. M., & Waddington, J. M. (2021). Mapping smouldering fire potential in boreal peatlands and assessing interactions with the wildland – human interface in Alberta, Canada. *International Journal of Wildland Fire*, *30*(7), 552–563. https://doi.org/10.1071/WF21001

Wilkinson, S. L., Moore, P. A., Flannigan, M. D., Wotton, B. M., & Waddington, J. M. (2018). Did enhanced afforestation cause high severity peat burn in the Fort McMurray Horse River wildfire? *Environmental Research Letters*, *13*(1). https://doi.org/10.1088/1748-9326/aaa136

Wilkinson, S. L., Moore, P. A., & Waddington, J. M. (2019). Assessing Drivers of Cross-Scale Variability in Peat Smoldering Combustion Vulnerability in Forested Boreal Peatlands. *Frontiers in Forests and Global Change*, *2*. https://doi.org/10.3389/ffgc.2019.00084

Wilkinson, S. L., Tekatch, A. M., Markle, C. E., Moore, P. A., & Waddington, J. M. (2020). Shallow peat is most vulnerable to high peat burn severity during wildfire. *Environmental Research Letters*, *15*. https://doi.org/10.1088/1748-9326/aba7e8

Wilkinson, S. L., Verkaik, G. J., Moore, P. A., & Waddington, J. M. (2020). Threshold peat burn severity breaks evaporation-limiting feedback. *Ecohydrology*, *13*(1). https://doi.org/10.1002/eco.2168

Wilson, C., Kampf, S. K., Wagenbrenner, J. W., & MacDonald, L. H. (2018). Rainfall thresholds for post-fire runoff and sediment delivery from plot to watershed scales. *Forest Ecology and Management*, *430*, 346–356. https://doi.org/10.1016/J.FORECO.2018.08.025

Wotton, B. M., Flannigan, M. D., & Marshall, G. A. (2017). Potential climate change impacts on fire intensity and key wildfire suppression thresholds in Canada. *Environmental Research Letters*, *12*(9). https://doi.org/10.1088/1748-9326/aa7e6e

Yochum, S. E. (2018). *Flow Resistance Coefficient Selection in Natural Channels: A Spreadsheet Tool*. https://www.fs.fed.us/biology/nsaec/assets/yochum2017flowresistancespreadsheettoolts-103-2.pdf

APPENDIX

Stochastic Precipitation and Potential Evapotranspiration Equations

A matrix of precipitation data is created in RHO using the following equation in MATLAB:

```
Precip = (random('Weibull',a,b,nod,noy) .*(rand(nod,noy)>0.27))./1000
```

where a random precipitation depth is chosen for each cell of the matrix from a Weibull distribution with a scale parameter (a) of 2.5 and a shape parameter (b) of 0.78, as specified by the first part of the equation. The second part of the equation randomly assigns which days receive their randomly assigned precipitation depth where on average 73% of days receive precipitation. Nod is the number of days of precipitation data that is being generated (or rows in the matrix) and noy represents the number of years of precipitation data being generated (or columns in the matrix). The values for a, b, and the average proportion of days that receive precipitation are based on average annual weather patterns for the Great Lakes region.

A matrix of potential evapotranspiration data is generated using the following equations. First a sinusoidal curve of the maximum PET possible for each day is created:

```
Ep=((Emax-Emin).*(0.5.*cosd((startDay*360/365:360/366:endDay*360/365)180)+0.5))'+ Emin
```

where E_{max} and E_{min} are the maximum PET values possible on the summer and winter solstices respectively (0.007 and 0.0005 m respectively for the purposes of this research). startDay and endDay are the Julien day of year for the start and end of the simulations. This array of maximum possible PET values is then repeated into a matrix with the number of columns equal to noy:

```
Ep = repmat(Ep,1,noy)
```

Next, a random value from an extreme value distribution is assigned to each day representing the proportion of the radiation which reaches the ground for non-rainy days:

```
cloudNR = random('ev',μ,σ,size(Ep))
```

where μ and σ are location and scale parameters with values 0.9 and 0.1 respectively. Any values that are greater than 1 are changed to be 1 and any values that are less than 0 are changed to be 0.

In a similar fashion a random value from a normal distribution is assigned to each day representing the proportion of radiation which reaches the ground for rainy days:

$$\text{cloudR} = \text{random}('\text{normal}',\mu,\sigma,\text{size}(\text{Ep}))$$

where μ and σ are the mean and standard deviation with values 0.5 and 0.2 respectively. Again, any values that are greater than 1 are changed to by 1 and any values that are less than 0 are changed to be 0.

Finally, using the already generated precipitation data the maximum possible PET values from the general sinusoidal curve are multiplied by the assigned value in cloudNR on days when precipitation is 0, and multiplied by the assigned value in cloudR when precipitation is greater than 0. The distributions for cloudNR and cloudR are based on cloud patterns from Northern Michigan, a region with similar climate and weather patterns compared to the study region.